



NATIONAL AND KAPODISTRIAN UNIVERSITY OF ATHENS

SCHOOL OF SCIENCE

DEPARTMENT OF INFORMATICS AND TELECOMMUNICATIONS

**MASTER'S PROGRAM IN
MICROELECTRONICS**

MASTER'S THESIS

**Simulation of nanoscale roughness evolution of Silicon
surfaces under Chlorine plasmas**

Iro-Maria C. Antoniou

Supervisor: George Kokkoris, Research Fellow, NCSR "Demokritos"

ATHENS

MARCH 2018



ΕΘΝΙΚΟ ΚΑΙ ΚΑΠΟΔΙΣΤΡΙΑΚΟ ΠΑΝΕΠΙΣΤΗΜΙΟ ΑΘΗΝΩΝ

**ΣΧΟΛΗ ΘΕΤΙΚΩΝ ΕΠΙΣΤΗΜΩΝ
ΤΜΗΜΑ ΠΛΗΡΟΦΟΡΙΚΗΣ ΚΑΙ ΤΗΛΕΠΙΚΟΙΝΩΝΙΩΝ**

**ΔΙΑΤΜΗΜΑΤΙΚΟ ΠΡΟΓΡΑΜΜΑ ΜΕΤΑΠΤΥΧΙΑΚΩΝ ΣΠΟΥΔΩΝ ΣΤΗ
ΜΙΚΡΟΗΛΕΚΤΡΟΝΙΚΗ**

ΔΙΠΛΩΜΑΤΙΚΗ ΕΡΓΑΣΙΑ

**Προσομοίωση εξέλιξης νανοτραχύτητας επιφανειών
Πυριτίου κατά την εγχάραξη με πλάσμα Χλωρίου**

Ηρώ-Μαρία Αντωνίου

Επιβλέπων : **Γεώργιος Κόκκορης**, Συνεργαζόμενος ερευνητής,
ΕΚΕΦΕ «Δημόκριτος»

ΑΘΗΝΑ

ΜΑΡΤΙΟΣ 2018

MASTER'S THESIS

Simulation of nanoscale roughness evolution of Silicon surfaces under Chlorine plasmas

Iro-Maria C. Antoniou
Registration Number.: MM227

SUPERVISOR: George Kokkoris, Research Fellow, NCSR "Demokritos"

March 2018

ΔΙΠΛΩΜΑΤΙΚΗ ΕΡΓΑΣΙΑ

Προσομοίωση εξέλιξης νανοτραχύτητας επιφανειών Πυριτίου κατά την εγχάραξη με πλάσμα Χλωρίου

Ηρώ-Μαρία Αντωνίου

A.M.: MM227

ΕΠΙΒΛΕΠΩΝ : **Γεώργιος Κόκκορης**, Συνεργαζόμενος ερευνητής, ΕΚΕΦΕ «Δημόκριτος»

Μάρτιος 2018

ABSTRACT

A surface model for Si etching by Cl₂ plasma is developed and coupled with a Monte Carlo (MC) modeling framework to predict the etching rate and the nanoscale roughness of Si surfaces. The surface model takes into account all etching mechanisms, i.e. ion-enhanced etching, physical sputtering, and pure chemical etching. However, under the conditions of the measurements and the pertinent calculations, ion-enhanced etching is dominant. Thus, a critical parameter for the accuracy of the calculations is the ion-enhanced etching yield (number of atoms of the substrate removed per incident ion).

The application of an etching yield expression from the literature to the MC framework leads to results which strongly deviate from etching rate measurements. The origin of the deviation is that the published expressions for the etching yield are phenomenological or “macroscopic”. The “macroscopic” etching yield captures the net effect of all surface processes, including redeposition of etching products and angle dependence of etching. This “macroscopic” etching yield is not suitable for a Monte Carlo framework which treats separately each surface process and not their net effect. For a Monte Carlo framework, a “nanoscopic” etching yield suitable to reproduce the “macroscopic” etching yield and rate is required. In this work, the “nanoscopic” etching yield of the dominant etching mechanism, namely ion-enhanced etching, is extracted by fitting the etching rate calculated by the MC framework to available measurements at ion energies of 100 eV. Then, the results of the MC framework are compared to measurements of etching rate and roughness for different values of the ion energy (50 to 500 eV).

The MC framework reproduces well the experimentally measured dependence of the etching rate on the ion energy. The etching rate is very close to the measurements up to ion energy of 300 eV and is overestimated for ion energies greater than 350 eV. This overestimation may be due a) to the assumption of a fully chlorinated surface which may not be valid at high ion energies and b) to the change of the composition of the ion flux arriving on the surface which is not taken into account. Regarding the root mean square (rms) roughness, although the absolute values are overestimated, the behavior of rms roughness versus ion energy is captured when the redeposition of the etching products is intense. The origin of the overestimation may be an underestimation of the sticking probability of ions on the surface.

SUBJECT AREA: Plasma etching

KEYWORDS: nanoscale surface roughness, Silicon, modeling, simulation, ion-enhanced etching, Monte Carlo

ΠΕΡΙΛΗΨΗ

Στην παρούσα εργασία αναπτύσσεται μοντέλο επιφανειακής χημείας που περιγράφει την εγχάραξη Πυριτίου σε πλάσμα Χλωρίου. Το μοντέλο ενσωματώνεται σε πλαίσιο προσομοίωσης Monte Carlo (MC) με στόχο την πρόβλεψη του ρυθμού εγχάραξης και της νανοτραχύτητας επιφανειών Πυριτίου. Στο μοντέλο λαμβάνονται υπόψη όλοι οι μηχανισμοί εγχάραξης, δηλαδή η υποβοηθούμενη από ιόντα εγχάραξη, η ιονοβολή καθώς και η χημική εγχάραξη. Ωστόσο, υπό τις συνθήκες των μετρήσεων και των υπολογισμών που παρουσιάζονται σε αυτή την εργασία, η υποβοηθούμενη από ιόντα εγχάραξη είναι ο κυρίαρχος μηχανισμός. Γι' αυτό και η κρίσιμη παράμετρος για την ακρίβεια των υπολογισμών είναι η απόδοση εγχάραξης της υποβοηθούμενης από ιόντα εγχάραξης (ο αριθμός των ατόμων του υποστρώματος που απομακρύνονται ανά προσπίπτον ιόν).

Η χρησιμοποίηση σχέσης από τη βιβλιογραφία για την απόδοση εγχάραξης οδηγεί σε αποτελέσματα που αποκλίνουν σημαντικά από τις πειραματικά μετρούμενες τιμές για το ρυθμό εγχάραξης. Η απόκλιση αποδίδεται στο γεγονός ότι οι σχέσεις για την απόδοση εγχάραξης που συναντώνται στη βιβλιογραφία είναι φαινομενολογικές ή «μακροσκοπικές». Η «μακροσκοπική» απόδοση εγχάραξης εμπεριέχει την καθαρή επίδραση από όλες τις επιφανειακές διεργασίες, συμπεριλαμβανομένων της επαναπόθεσης των προϊόντων εγχάραξης και της γωνιακής εξάρτησης της εγχάραξης. Η «μακροσκοπική» απόδοση εγχάραξης δεν αποτελεί ορθή επιλογή για το πλαίσιο προσομοίωσης MC που διαχειρίζεται ξεχωριστά κάθε επιφανειακή διεργασία και όχι την καθαρή επίδρασή τους. Για το πλαίσιο MC απαιτείται μία «νανοσκοπική» απόδοση εγχάραξης η οποία θα αναπαράγει τη(ο) «μακροσκοπική(ό)» απόδοση (ρυθμό) εγχάραξης. Στα πλαίσια της παρούσας εργασίας, η «νανοσκοπική» απόδοση εγχάραξης του κυρίαρχου μηχανισμού εγχάραξης προκύπτει από προσαρμογή του ρυθμού εγχάραξης που υπολογίζεται από το πλαίσιο Monte Carlo σε διαθέσιμες από πειράματα μετρήσεις για ενέργεια ιόντων ίση με 100 eV. Στη συνέχεια, γίνεται σύγκριση των αποτελεσμάτων του πλαισίου με μετρήσεις του ρυθμού εγχάραξης και της τραχύτητα σε εύρος ενέργειας ιόντων 50 με 500 eV.

Το πλαίσιο MC αναπαράγει επιτυχώς την πειραματικά μετρούμενη εξάρτηση του ρυθμού εγχάραξης από την ενέργεια ιόντων για ενέργειες μέχρι περίπου 300 eV. Ο ρυθμός εγχάραξης υπερεκτιμάται για ενέργειες ιόντων υψηλότερες των 350 eV. Αυτή η υπερεκτίμηση μπορεί να οφείλεται α) στην παραδοχή πλήρως χλωριωμένης επιφάνειας που ενδέχεται ωστόσο να μην ισχύει στις περιπτώσεις των υψηλών ενεργειών ιόντων και β) στην αλλαγή της σύστασης των ιόντων που φθάνουν στην επιφάνεια η οποία δε λαμβάνεται υπόψη. Όσον αφορά στην rms (root mean square) τραχύτητα, αν και οι απόλυτες τιμές υπερεκτιμώνται, η συμπεριφορά της rms τραχύτητας συναρτήσει της ενέργειας των ιόντων ακολουθεί τις μετρήσεις στην περίπτωση όπου το φαινόμενο της επαναπόθεσης των προϊόντων εγχάραξης είναι έντονο. Η υπερεκτίμηση αυτή μπορεί να οφείλεται σε υποεκτίμηση της πιθανότητας προσκόλλησης των ιόντων στην επιφάνεια.

ΘΕΜΑΤΙΚΗ ΠΕΡΙΟΧΗ: Εγχάραξη με πλάσμα

ΛΕΞΕΙΣ ΚΛΕΙΔΙΑ: τραχύτητα σε νανοκλίμακα, Πυρίτιο, μαθηματική προτυποποίηση, προσομοίωση, εγχάραξη υποβοηθούμενη από ιόντα, Μόντε Κάρλο

CONTENTS

| | |
|--|-----------|
| PROLOGUE | 11 |
| 1. INTRODUCTION | 12 |
| 1.1 Challenges of plasma etching..... | 12 |
| 1.2 The importance of surface roughness in microelectronics and other fields..... | 12 |
| 1.3 Plasma etching mechanisms | 12 |
| 1.4 Roughness of Silicon surfaces: Evidence, mechanisms, and control | 14 |
| 1.5 Literature review of the methods used for the evolution of the surface morphology | 16 |
| 1.6 The purpose of the thesis..... | 18 |
| 2. THE MODELING FRAMEWORK FOR THE EVOLUTION OF SILICON SURFACE MORPHOLOGY UNDER CHLORINE PLASMA ETCHING | 19 |
| 2.1 Introduction..... | 19 |
| 2.2 Surface model for Si etching by Cl ₂ plasma | 19 |
| 2.2.1 The gas phase of Cl ₂ plasma | 19 |
| 2.2.2 Surface processes | 20 |
| 2.3 Monte Carlo framework for the evolution of surface morphology | 26 |
| 2.3.1 Basic concepts of the framework [19] | 26 |
| 2.3.2 The simulation procedure..... | 26 |
| 2.3.3 Surface morphology characterization | 27 |
| 2.3.4 Time and space dimensions | 28 |
| 3. RESULTS..... | 31 |
| 3.1 Introduction..... | 31 |
| 3.2 Case study | 32 |
| 3.3 The effect of the dimensions of the surface on the calculated etching rate and rms roughness | 33 |

| | | |
|-----|--|----|
| 3.4 | The effect of the dimensions of the unit cell on the calculated etching rate and rms roughness | 34 |
| 3.5 | First comparison of the calculated etching rate with measurements | 35 |
| 3.6 | Extraction of “nanoscopic” values of the parameter defining the ion-enhanced etching yield | 36 |
| 3.7 | Extraction of “nanoscopic” values of the parameter defining the physical sputtering yield | 38 |
| 3.8 | Comparison of model results with measurements of etching rate and rms versus the ion energy | 39 |
| 4. | CONCLUSIONS..... | 41 |
| | REFERENCES | 43 |

LIST OF FIGURES

| | |
|--|----|
| Figure 1.1 a) Sidewall roughness – roughness on the sidewalls of trenches of polymeric lines [Scanning electron microscope (SEM) image]. b) Open area surface roughness of a Si surface (SEM image) [23]..... | 14 |
| Figure 2.1 The curves coming from equation 2.1 for $R = 200$ and from equation 2.3 for $\sigma = 0.05$ rad are identical..... | 20 |
| Figure 2.2 The functions $f_{Si}(\theta)$ (equation 2.13 and equation 2.11) demonstrating the dependence of physical sputtering and ion-enhanced etching yield of Si on the angle of ion (Ar^+) incidence, θ . The parameters a_0 , ϕ_1 , and ϕ_2 of equation 2.13 are also noted..... | 24 |
| Figure 2.3 Cl^+ sticking probability on $SiCl_x(s)$ ($x=0,1,2,3$, and 4)..... | 25 |
| Figure 2.4 Ion energy functions of the etching yield expressions (from equations 2.10 and 2.12) for $A_{SiCl_x} = 0.353 \text{ eV}^{-0.5}$ [54] and $A_{Si} = 0.0356 \text{ eV}^{-0.5}$ [46]..... | 25 |
| Figure 2.5 Schematic with the inputs and the outputs of the MC modeling framework..... | 26 |
| Figure 3.1 a) Etching rate and b) rms roughness of Si surfaces under Cl_2 plasma measured by Nakazaki et al. [23]..... | 31 |
| Figure 3.2. a) The etching rate (average value of 6 runs per case) and b) the rms roughness (average value of 6 runs per case) versus time for surfaces with different dimensions, i.e. $512 \times 512 \text{ nm}^2$, $256 \times 256 \text{ nm}^2$, $128 \times 128 \text{ nm}^2$, and $64 \times 64 \text{ nm}^2$. The results correspond to cases 0001 to 0004 of Table 3.I..... | 34 |
| Figure 3.3. a) The etching rate (average value of 6 runs) and b) the rms roughness (average value of 6 runs) for an $128 \times 128 \text{ nm}^2$ surface and unit cell dimensions of 1 nm^3 , 0.5853 nm^3 and 0.2713 nm^3 . The results correspond to cases 0003, 0005, and 0006 of Table 3.I..... | 35 |
| Figure 3.4. The etching rate (average value of 3 runs) for an $128 \times 128 \text{ nm}^2$ surface and unit cell dimensions of 0.271 nm^3 . The results for two cases (cases 0007 and 0008 of Table 3.I) are shown. In the first case, the parameters of the surface model are taken from Tsuda et al. [54,56] are used. In the second case, no angle dependence of the etching yield and no redeposition of etching products are considered, i.e. $f_{SiCl_x}(\theta)=1$ (see equation 2.10) and $S_d=0$ | 36 |
| Figure 3.5 a) The etching rate and b) the rms roughness vs the ion energy as obtained from our simulation and the measurements of Nakazaki et al. [23]. The simulation results refer to cases 0014 to 0029: Two values of S_d are considered: $S_d=0.05$ and $S_d=1$. The error bars are coming from the standard deviations of the runs of each case..... | 40 |

LIST OF TABLES

| | |
|---|----|
| Table 2.I. Surface processes during etching of a Si surface with a Cl ₂ plasma [54]..... | 20 |
| Table 3.I The values of the parameters used for the runs. The total etching time is 120 s for all cases. A_{SiCl_x} and A_{Si} are the parameters defining the ion-enhanced and physical sputtering yield (see equations 2.10 and 2.12), a_{chem} is the coefficient of pure chemical reaction of a saturated (with Cl) Si surface, x_+ is the fraction of ions in the arriving flux, S_d is the sticking probability of the etching products, E_+ is the ion energy, $f_{SiCl_x}(\theta)$ is the function defining the angle dependence of the ion-enhanced etching yield (see equation 2.11)..... | 33 |
| Table 3.II The “nanoscopic” values of A_{SiCl_x} (in eV ^{-0.5}) and S_d reproducing the experimental value of the etching rate for an ion energy equal to 100 eV (~260 nm/min) and for different values of S_d . The value proposed by Tsuda et al. [56] is 0.353 eV ^{-0.5} | 37 |
| Table 3.III The values of rms in nm for the “nanoscopic” values of A_{SiCl_x} and S_d from Table 3.II. | 38 |
| Table 3.IV The “nanoscopic” values of A_{Si} reproducing the “macroscopic” value of the physical sputtering rate (19.4 nm/min, ions at 100 eV with a flux of 10 ²⁰ m ⁻² s ⁻¹) | 39 |

PROLOGUE

Such an interesting journey meets its end, or not? This step is the first of a longer journey. I would like to thank all my companions during this fascinating journey and period of my life. First of all, my family, as without their support, I simply wouldn't have made it. Secondly, all my tutors in MSc Microelectronics who patiently and effectively built my knowledge basis in microelectronic engineering. To continue, all my fellow students, by interacting with whom I gained better understanding of the field of microelectronics. I wish them all the best. And finally, I would like to thank my tutor and supervisor, Mr. George Kokkoris, for his patience, collaboration, scientific and emotional support during the production of my thesis.

The thesis was held at the Institute of Nanoscience and Nanotechnology (INN) of NCSR Demokritos. Computers from the computer cluster "Nessie" of INN were utilized for the implementation of the simulation.

1. INTRODUCTION

1.1 Challenges of plasma etching

Due to the fact that device dimensions are continuously scaling down to tens of nanometers (nm), the importance of plasma-induced surface roughness in modern microelectronic devices increases. The precision in profile control, critical dimension (CD), selectivity, and damage becomes more demanding. The major challenges of etching during pattern transfer are [1] a) mask erosion, b) deviations from vertical sidewalls, c) mask undercutting, d) mask roughness transferred to the film being etched inducing line edge and line width roughness (LER and LWR), e) notching, f) microtrenching, g) etching lag and inverse etching lag, and h) microloading.

1.2 The importance of surface roughness in microelectronics and other fields

Surface roughness is a usual outcome of the micro- and nanofabrication processes (see Section 1.3) and can be critical for several applications and pertinent fields. In some of them, roughness is an artifact to be eliminated and in other, it is a useful property of the surface.

Firstly, **it is important in micro- and nanoelectronics**. Roughness on atomic- or on nanoscale deeply affects device operation as it is of the same scale as the critical dimension (CD) of the etched features [1]. In particular, the line edge roughness (LER), i.e. the roughness addressing the fluctuations of a line edge about its mean value, and the consequent line width roughness (LWR), i.e. the fluctuations in a linewidth about its mean value [2], may induce performance variability or even destabilize the performance of the transistor. Both the gate length and the threshold voltage may be affected [2, 3].

It is also important in microelectromechanical systems (MEMS). Even though the scale is larger, roughness has an impact on the fracture strength of microstructures and the friction between moving parts. In Silicon (Si) MEMS fabrication, surface forces may make the surface permanently adhesive and friction between contacting surfaces may appear as a result of large surface-to-volume ratio and low loads [4, 5]. Surface roughness with positive skewness and high kurtosis at the contact interfaces, as well as induction of asymmetry and peakiness is reducing the adhesive and friction effects [4].

Roughness also affects the wetting properties of the surfaces. Surfaces presenting roughness at the micro- and/or the nanoscale can become super-hydro(oleo)phobic [6, 7].

Nanoroughness can enhance the antireflectivity not only for Si, but also for polymeric surfaces [8].

Roughness can also be critical for the interaction of surfaces with biological samples. Protein adsorption on surfaces is affected by the surface roughness [9, 10].

With a level of periodicity, the surface roughness, can be useful to magnetic storage [11], catalysis [12], and nano-patterning [13].

1.3 Plasma etching mechanisms

The origin of surface roughness during plasma etching of Si or other substrates is attributed to competitive “forces” between roughening and smoothing and comes from

the non-uniformity of the etching rate on the surface of the substrate. Thus, it is useful to identify the etching mechanisms in a plasma environment.

First of all, etching techniques are separated into wet and dry or plasma etching techniques. Wet etching is more a chemical than a physical process. It is therefore, quite a selective and isotropic process. Plasma etching allows for both anisotropic and isotropic etching depending on the conditions and the dominant mechanism. Plasma etching can be categorized to chemical etching, physical sputtering, and ion-enhanced etching.

Chemical etching is attributed to highly reactive neutral species chemically sensitive with specific substrates, i.e. F with Si or Cl₂ with Al [14]. It is a selective mechanism which leads to isotropic etching. The etching rate in this case follows the Arrhenius relation,

$$ER_{ch} = k_0 \exp\left(-\frac{E_a}{kT}\right)Q \quad (1.1)$$

with Q being the reactive species flux, k_0 the pre-exponential factor, and E_a is the activation energy.

Physical sputtering is the ejection of atoms or molecules from the surface due to energetic ion bombardment [15]. Sputtering is an unselective process since the sputtering yield (number of substrate atoms removed per incident ion) depends only on the ion energy, the surface binding energy, and the masses of the targets and projectiles. The latter two parameters do not vary by more than a factor of 2-3 among different materials [15]. Sputtering is also an anisotropic process strongly sensitive to the angle of the incidence of the ion. The etching yield of physical sputtering reads [14, 16]

$$EY_{PS} = A_{PS} \left(\sqrt{E_+} - \sqrt{E_{th}} \right) f(\theta) \quad (1.2)$$

where E_{th} is the threshold energy for physical sputtering, A_{PS} depends on the ion-substrate combination (in particular, on the surface binding energy, and the masses of the targets and projectiles), and $f(\theta)$ is a function which expresses the dependence of the etching yield on the angle of incidence of the ion, θ .

Last but not least, **ion-enhanced** (chemical) **etching** occurs when a target substrate is exposed to both reactive neutrals and ion bombardment. Among plasma etching mechanisms, ion-enhanced etching is the most promising for micro- and nanofabrication and essentially interesting for this thesis also. Ion-enhanced etching was introduced by Coburn and Winters [17]. They observed that the etching rate in the case of Si containing substrate (Si, SiN₃, SiO₂, SiC) etching under beams of XeF₂ and Ar⁺ is higher than the etching rate by an XeF₂ or Ar⁺ beam alone. They proposed that **synergistic etching** occurs under the simultaneous bombardment of the surface by XeF₂ and Ar⁺ beams, as they measured etching rates an order of magnitude greater than in physical sputtering (Ar⁺ beam alone).

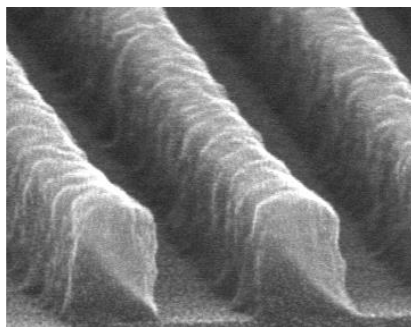
In ion-enhanced etching, the ion bombardment boosts one of the steps of the chemical etching process, e.g. the surface adsorption, the etching reaction itself or the byproduct

removal. For example, the ion bombardment causes damage (breaking bonds, etc.) which makes the surface more apt to chemically react with the radical. Alternatively, the ion bombardment may dislodge or sputter away etch byproducts which would otherwise tend to stay on a surface and impede the etching process [18]. Ion enhanced etching is an anisotropic etching process usually with a much greater rate compared to physical sputtering. Selectivity is also better compared to physical sputtering. The etching yield for ion-enhanced etching depends on the ion energy as the etching yield for physical sputtering; it is also angle dependent.

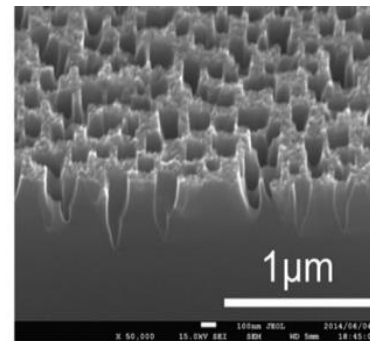
Besides, the three mechanisms of material removal, simultaneous deposition may occur during plasma etching [19, 20]. Depositing species, or “etch-inhibitors”, coming from the reactions on the etched surface (product redeposition), the chemical reactions in the bulk of the plasma reactor, and the etching of the inner surface of the plasma reactor, are deposited on the etched surface, play the role of etching masks, and induce roughness on the etched surface.

1.4 Roughness of Silicon surfaces: Evidence, mechanisms, and control

Surface roughness may be formed either on the sidewall (Figure 1.1a) of the etched feature (e.g. trench or hole), or on open areas samples (Figure 1.1b). In the first case we refer to sidewall roughness which contributes to LER and LWR. Both the direct interaction of the plasma with the sidewall (during the pattern transfer step) and the shadowing of the ion flux by the overlying mask [21, 22] contribute to the formation of sidewall roughness. In the second case, i.e. in the case of open area samples, the roughness comes only from the interaction of the plasma with the surface of the samples.



(a)



(b)

Figure 1.1 a) Sidewall roughness – roughness on the sidewalls of trenches of polymeric lines [Scanning electron microscope (SEM) image]. b) Open area surface roughness of a Si surface (SEM image) [23].

The focus of this work is on the formation of surface roughness during plasma etching of open area Si substrates. There are a few previous works investigating the factors affecting the roughness formation. In particular, Petri et al. [24] presented a parametric study of single-crystal Si roughness induced by a Sulfur hexafluoride (SF_6) plasma in a helicon source reactor. The aim was to study the effect of several operating parameters, i.e. the ion flux (J_+) and energy (E_+), the flux of neutral species (J_F), and the etching time (t), on the surface roughness. They came up with an empirical relation for root mean square (rms) roughness [24, 25]

$$\text{rms} \propto \frac{1}{\sqrt{E_+}} \left(\frac{J_+}{J_F} \right)^{0.45} t \quad (1.3)$$

At low ion flux the surface is smoothed by the neutral species, while at higher ion flux, the neutral species roughen the surface as ion induced effects are triggered [24].

Hwang et al. [26] studied the evolution of surface roughening of Si (as well as of other substrates) during etching by Chlorine (Cl_2) plasma. The outcome of the study was that the surface roughness depended on self-bias voltage and pressure. The rms roughness increased with pressure (10 – 30 mTorr) and decreased with self-bias voltage (100 – 250 V) for Si whose boiling temperature of by-products is low, whereas the rms decreased with pressure and increased with bias voltage during etching of other substrates, i.e. Hafnium Nitride (HfN) and Iridium Oxide (IrO_2), whose boiling temperature of by-products is high. It was understood that the contrasting trends from the experimental results originated from the different volatility of the etch by-products which were generated during etching in Cl_2 . It was also observed that, when bias voltage and pressure varied, surface roughness was inversely proportional to the etching rate during etching of Si, while surface roughness was proportional to the etching rate of HfN and IrO_2 . In addition, it was found that surface roughness increased as a function of the etching time.

Sung and Pang [27] studied Si etching with Cl_2 plasma generated by a multipolar electron cyclotron resonance source by means of mass spectroscopy, optical emission spectroscopy, and atomic force microscopy (AFM). They reported that both the etching rate and the surface roughness of Si samples increased with the increase of the rf power on the electrode.

Kokkoris et al. [20] and Boulousis et al. [28] investigated the effect of the etching time and wafer temperature on the surface roughness of Si during etching with SF_6 plasma in a helicon type reactor. The plasma etched surfaces were analyzed by AFM. Dual nanoscale morphology, as well as, almost linear increase of both rms roughness and correlation length versus etching time was observed in the experiment. The rms roughness decreased with the wafer temperature. A mechanism based on the deposition of etch-inhibitors (coming either from the reactor dome or the clamping ring of the electrode or the reactor walls) during the etching process was proposed for the explanation of the experimental behavior. In addition, appropriately designed experiments were conducted [8, 28] and confirmed the proposed mechanism.

Yin & Sawin [29] measured the evolution of roughness of Si surfaces in Argon (Ar) plasma by AFM as a function of ion bombardment energy, ion impingement angle, and etching time in an inductively coupled plasma beam chamber. In this chamber, the plasma chemistry, ion energy, ion flux, and ion incidence angle can be adjusted independently. Their study demonstrated the importance of the angle of ion incidence on the surface roughness. Very small values of roughness were observed for normal angle of ion incidence. The roughness became greater at grazing angles. In particular, a striation structure was formed at grazing angles which was either parallel or transverse to the beam impingement direction depending on the off-normal angle.

Martin & Cunge [30] analyzed the roughness generated on c-Si (100) surfaces when etched in an inductively coupled industrial plasma source over a wide range of conditions, i.e. pressure and rf power, and using SF_6 , CF_4 , Cl_2 , and HBr chemistries. They reported that plasma etching did not induce roughness on the Si surface; on the

contrary, it smoothed the Si surface, if surface roughness initially existed. Given that in high density plasmas the local etch rate is generally limited by the availability of reactive radicals, the smoothing was attributed to the fact that the hills of a rough surface received a higher flux of etchant radicals than the valleys. Finally, the authors showed that the roughening of Si in F-based plasmas was only due to the micromasking of Si by AlF_x particles originating from the sputtering of the reactor walls which were made by Alumina (Al_2O_3). However, when the chamber walls were intentionally coated by a carbon layer prior to the Si etching process, the F-based plasmas behaved like the other etching chemistries investigated: they rapidly smoothed any existing roughness.

Nakazaki et al. [23] reported two surface evolution modes during Si etching in inductively coupled Cl_2 plasmas, i.e. the roughening and the smoothing mode. These modes depend upon the ion energy, E_+ : At $E_+ < 200 - 300$ eV, the rms roughness is almost linearly dependent on time, whereas at $E_+ > 200 - 300$ eV, it is lowered and presents a 'quasi-steady state' most of the etching time. The transition from the roughening to the smoothing mode is attributed to a change in the gas species as the ion energy increases. In particular, Cl_x^+ ions, the dominant species at lower energies, are subsided by $SiCl_x^+$ ions, originating from the increased production of etching products, at higher energies.

A means to reduce and control surface roughness of Si is atomic layer etching (ALE) [31] which consists of a step of surface modification (formation of a $SiCl_x$ layer) and a subsequent step of Ar^+ ion bombardment with suitable energy (~50 eV). Continuous plasma etching simultaneously exposes the surface to energetic Ar^+ , as well as reactive ions such as Cl^+ and Cl_2^+ that are similarly energetic as the Ar^+ . Energetic reactant ions **damage Si as they break Si-Si surface bonds**, thus allowing Cl atoms to diffuse and alter the lattice structure. Accumulated surface roughness occurs with the strong Si-Cl bonding that produces a high activation barrier for surface diffusion and prevents flattening of the silicon surface. In ALE, the difference is that the removal step does not involve reactive chlorine ions because chlorine is not intentionally present. Although energetic Ar^+ can break Si-Si bonds, at Ar^+ energy values well below the sputtering threshold, these bonds can reform once the chlorine bonds are removed. This smoothing or resetting effect in Si ALE is thus attributed to the higher surface atom mobility under Ar^+ bombardment at suitable ion energies.

1.5 Literature review of the methods used for the evolution of the surface morphology

The methods for the evolution of surface morphology entail a discrete or a continuum description of the surface morphology (or profile) and a Monte Carlo model or a deterministic method for the surface (or profile) evolution. The **string method** [32, 33], the **method of characteristics** [34-36], and the **level-set method** [37-40] are deterministic algorithms for the evolution of the surface morphology; in all these algorithms, the description of the surface morphology is continuum. The **cell-based method** [19, 41-43] is a stochastic algorithm based on a Monte Carlo model and the description of the surface morphology is discrete.

In the string method, in 2 dimensions (2d) the profile is visualized by a string of nodes and straight line segments connecting the nodes [1]. Every node is moved vertically to the moving boundary following the local boundary velocity and the equation of movement. Difficulty is encountered at sharp corners, where the points at the corner advance faster than those on the sidewall and cause unrealistic lateral retraction [1].

Challenges arise as the step size must be kept small so as to avoid the formation of loops. In 3 dimensions (3d), difficulties occur regarding the detection of triangular intersections and delooping. In the method of characteristics, an improvement of the string method, the node trajectory is allowed to lean in different directions dependent upon the etching rate [1]. The level-set method is based upon the concept of the implicit function. The evolving profile or surface is defined as the zero level set of the implicit function [44]. Last but not least, in the cell-based method, the surface morphology consists of cubic cells each of which may contain more than one atom or molecule (coarse graining). Cells can be removed or added depending on etching or deposition probabilities as defined by the etching yields and the sticking probabilities.

In this work, we utilized a cell-based method, a cell-based framework to study the evolution of surface morphology of Si substrates in Cl₂ plasmas. A review of the cell-based frameworks is following.

Sawin and coworkers developed a 3d modeling framework for polysilicon etching in inductively coupled Cl₂ and HBr plasmas [45-47]. The cell size is comparable to the halogenation length (in halogen-based plasma etching) [46, 47]. They claimed that a “continuous surface must be generated from the surface cells rather than using the faces of the surface cells to accurately compute the surface kinetics” [1]. Regarding the surface normal calculation, 4 or 6 neighboring cells are taken into account [45]. They developed a “mixing-layer kinetics model” [46] considering vacancies among species. They investigated the onset of surface roughening and reported that the angle of ion incidence onto the surface was a key parameter for determining the perpendicular and parallel ripples.

Kushner and coworkers [43, 48-50] developed a 3d profile simulator for feature scale profile evolution and applied it in several cases of feature etching; they also coupled the profile simulator with a reactor scale module.

Wang and coworkers [51, 52] developed a (2+1)d Monte Carlo simulation framework to study the scaling behavior of plasma etching of Si substrates. They concluded that the method used for the determination of the surface normal did not affect the scaling behavior. The eight closest in-plane neighbors were finally considered for the determination of the surface normal. A critical assumption of their model was a higher sticking coefficient for the reemitted than the incident flux.

Ono, Eriguchi, and coworkers [42, 53-56] started from (1+1)d and finally developed a 3d profile evolution simulator and applied it in Si etching in chlorine-based plasmas. The redeposition of etch products and byproducts were taken into account. Surface roughness was calculated as a function of ion energy (or rf bias) and other parameters. The surface normal was calculated by taking into account 5 x 5 x 5 cells surrounding the cell of incidence. Agreement with measured values was observed for ion energies up to 250 eV. The effect of several parameters such as the angle of ion incidence is investigated.

Kokkoris et al. [19, 20] developed a (2+1)d Monte Carlo simulation framework and studied the effect of ‘simultaneous-to-etching deposition’ (SIMED) on the surface morphology evolution. The role of etch-inhibitors coming from the reactor walls and/or produced in the reactor bulk on the roughness of Si [20] and polymeric surfaces [13] is investigated. The presence of etch-inhibitors was found to contribute to the formation of periodic dots on the etched surface [19].

1.6 The purpose of the thesis

The purpose of the thesis is the development of a surface model for Si etching under Cl_2 plasma. The surface model will be incorporated in an available Monte Carlo modeling framework [19] in order to calculate the evolution of nanoscale roughness of Si surfaces. The Monte Carlo framework will be extended to properly treat the ion-enhanced etching mechanism, which is dominant in etching of Si with Cl_2 plasma. The coupling of the surface model with the Monte Carlo framework will be evaluated by a comparison to measurements [23] of the etching rate and roughness versus the ion energy.

A Monte Carlo modeling framework coupled with a validated surface model is a very useful tool for the prediction of nanoscale roughness of plasma etched surfaces. As the dimensions of integrated circuits and electronic devices are continuously decreasing according to the International Technology Roadmap of Semiconductors (ITRS) 2015, nanoscale roughness has a continuously bigger impact on the fabrication processes and the properties of fabricated surfaces. The modeling framework can shed light on the mechanisms of roughness formation and evolution and contribute to the design of recipes delivering the desired (per application) surface roughness.

2. THE MODELING FRAMEWORK FOR THE EVOLUTION OF SILICON SURFACE MORPHOLOGY UNDER CHLORINE PLASMA ETCHING

2.1 Introduction

The study of roughness formation and evolution of Si surfaces during etching in Cl₂ plasmas requires a) a Monte Carlo (MC) framework [19] where the surface morphology is represented by a matrix of cubic cells and b) a surface model for Si etching by Cl₂ plasma which describes the surface processes during etching. The surface model is based on a surface model reported by Tsuda et al. [54-56] and is described in Sec. 2.2. The MC framework is described shortly in Sec. 2.3 and in detail in Ref. [19].

2.2 Surface model for Si etching by Cl₂ plasma

2.2.1 The gas phase of Cl₂ plasma

A series of charged and neutral species are produced in the reactor bulk of a Cl₂ plasma [54]. The most critical species for the etching of Si surfaces, i.e., energetic chlorine ions (Cl⁺) and atomic chlorine (Cl), are considered to join the surface processes. Cl⁺ ions are considered mono-energetic ($E_+ = 100$ eV in the base case) and follow a Gaussian angular distribution around a basic angle. The standard deviation of the Gaussian angular distribution is related to the ratio $E_+/(kT_+)$, where E_+ is the ion energy and kT_+ is the ion temperature in eVs (k is the Boltzmann constant). Tuda et al. [57] used the equation 2.1 to describe the angular distribution of ions after passing through a collisionless sheath; the ions enter the sheath with a Maxwellian velocity distribution function.

$$G_+(\theta) = \frac{\exp(R)}{\sqrt{\pi}} \left[\frac{\sqrt{R} \sec \theta \exp(-R^2 \sec^2 \theta) + \frac{\sqrt{\pi}}{2} \operatorname{erfc}(\sqrt{R} \sec \theta)}{2} \right] \cos \theta, \quad (2.1)$$

where

$$\operatorname{erfc}(x) = \frac{2}{\sqrt{\pi}} \int_x^\infty \exp(-t^2) dt. \quad (2.2)$$

θ is the incident angle of ions and R is the ratio $E_+/(kT_+)$ (the ion energy in the model of Tuda et al. [57] was considered equal to the sheath potential). Equation 2.1 was utilized by several subsequent works [56, 58]. The curves coming from equation 2.1 for different values of R are fitted to Gaussian angular distributions, i.e.,

$$G_+(\theta) = \frac{1}{\sigma\sqrt{2\pi}} \exp \left[-\frac{1}{2} \left(\frac{\theta}{\sigma} \right)^2 \right] \quad (2.3)$$

with different standard deviations, σ . Curves coming from both equations 2.1 and 2.3 are shown in figure 2.1. Cl atoms follow an isotropic (cosine) angular distribution and their temperature (gas temperature) is T_g .

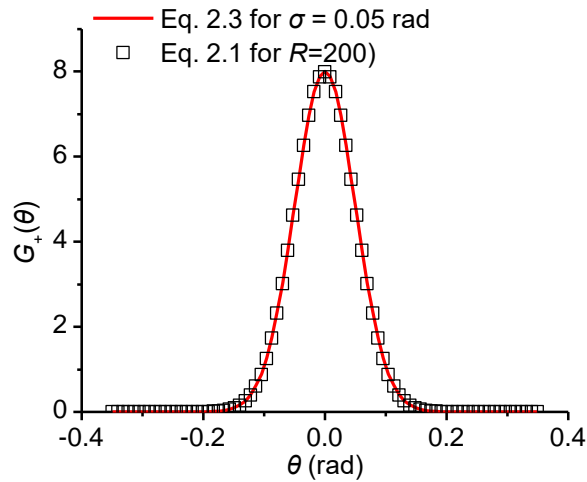


Figure 2.1 The curves coming from equation 2.1 for $R = 200$ and from equation 2.3 for $\sigma = 0.05$ rad are identical.

2.2.2 Surface processes

The mechanisms of etching of Si in a Cl_2 plasma are a) physical sputtering, b) ion-enhanced (chemical) etching, and c) pure chemical etching. Besides the species from the gas phase (see section 2.3.1), the species joining the surface etching model are adsorbed chlorine species ($\text{SiCl}_x(\text{s})$, $x=1,2,3,4$), saturated (SiCl_4) and unsaturated (SiCl_x , $x=1,2,3$) etching products. The surface processes during etching of Si surfaces with Cl_2 plasmas are described in Table 2.I.

Table 2.I. Surface processes during etching of a Si surface with a Cl_2 plasma [54].

| | Reaction | Process | | Coefficient |
|---|-------------------------------|--|------------------|------------------------|
| 1 | Adsorption of neutral species | $\text{SiCl}_x(\text{s}) + \text{Cl}(\text{g}) \rightarrow \text{SiCl}_{x+1}(\text{s})$ | $x = 0, 1, 2, 3$ | S_x |
| 2 | Chemical etching | $\text{SiCl}_3(\text{s}) + \text{Cl}(\text{g}) \rightarrow \text{SiCl}_4(\text{g})$ $\text{SiCl}_4(\text{s}) \rightarrow \text{SiCl}_4(\text{g})$ | | α_{chem} |
| 3 | Ion enhanced etching | $\text{SiCl}_x(\text{s}) + \text{Cl}^+ \rightarrow \text{SiCl}_x(\text{g})$ | $x=1,2,3,4$ | EY_{SiCl_x} |
| 4 | Physical sputtering | $\text{Si}(\text{s}) + \text{Cl}^+ \rightarrow \text{Si}(\text{g})$ | | EY_{Si} |
| 5 | Redeposition | $\text{SiCl}_x(\text{g}) \rightarrow \text{SiCl}_x(\text{s})$ | $x=0,1,2,3,4$ | S_d |

The first of the surface processes (reaction 1 in Table 2.I) is the adsorption of Cl on the Si surface. The coefficient of this reaction, or the effective sticking coefficient, is assumed to depend on the chlorination level of the surface in some works [54, 56],

while in other works it is assumed to be equal to 1 [55] on unsaturated Si surface. In this work, we consider that

$$S_x = 1, \quad (2.4)$$

where $x=0,1,2,3$. When x is equal to 4, i.e. the surface is saturated with chlorine, no more adsorption takes place. If Cl is not adsorbed on the surface, it is diffusively reemitted from the surface. The temperature (energy) of the reemitted Cl from the surface is equal to the surface temperature, T_s . It has to be noticed that x increases not only with the impact of a Cl atom but also with the impact of Cl^+ ion. In this case, the energy of the reemitted Cl atom is the energy of the ion.

At the last step of chlorination process, pure chemical (reaction) etching can occur (reaction 2 in Table 2.1) producing volatile product $SiCl_4$. The calculation of this coefficient (a_{chem}) can be based on the expression of Ogryzlo et al. [59] for the etching rate, i.e.

$$ER = \nu N_e^\gamma n_{Cl} \sqrt{T_s} e^{-E/(kT_s)} \quad (2.5)$$

where n_{Cl} is the number density of Cl atoms, T_s is the surface temperature, N_e is the doping concentration of Si, and E is the activation energy. The values of all parameters of equation 2.5, including ν and γ , were extracted by Ogryzlo et al. by fitting of equation 2.5 to measurements for Si surface with different orientation and doping levels [59].

The etching rate can be also formulated as

$$ER = \frac{a}{d_{Si}} \frac{1}{4} n_{Cl} u_{Cl} \quad (2.6)$$

where

$$u_{Cl} = \sqrt{\frac{8kT_g}{\pi m_{Cl}}} \quad (2.7)$$

is the thermal speed of Cl atoms. T_g is the gas temperature, and m_{Cl} is the mass of Cl atoms. d_{Si} in equation 2.6 is Si number density. The coefficient a expresses the probability for chemical reaction, i.e. the production of volatile $SiCl_4$, when Cl atom flux arriving on the Si surface. This coefficient should incorporate all sticking probabilities during successive chlorination of the surface as well as coefficient a_{chem} of pure chemical reaction of saturated Si surface, i.e. a surface where $SiCl_4(s)$ has been formed. a can be formulated as

$$a = S_0 S_1 S_2 S_3 a_{chem}, \quad (2.8)$$

where S_x is coming from equation 2.4. By combining equations 2.5 – 2.8, a_{chem} reads

$$a_{\text{chem}} = \frac{16d_{\text{Si}}vN_e^y\sqrt{T_s}e^{-E/(kT_s)}}{S_0S_1S_2S_3\sqrt{\frac{8kT_g}{\pi m_{\text{Cl}}}}} \quad (2.9)$$

Besides chlorination and chemical etching, Cl^+ ions can induce ion-enhanced etching (reaction 3 of Table 2.I) and physical sputtering (reaction 4 of Table 2.I) of the Si surface. The etching yield for ion-enhanced etching depends on the ion energy, the angle of ion incidence, and the chlorination level, and reads [23, 54, 60]

$$EY_{\text{SiCl}_x} = \frac{\chi}{4} A_{\text{SiCl}_x} \left(\sqrt{E_+} - \sqrt{E_{\text{th,SiCl}_x}} \right) f_{\text{SiCl}_x}(\theta), \quad (2.10)$$

where $E_{\text{th,SiCl}_x}$ is the threshold energy for ion-enhanced etching (12 eV) [55] and θ is the incident angle of ions (rads). The function f_{SiCl_x} reads [46, 54, 61]

$$f_{\text{SiCl}_x}(\theta) = \left\{ \begin{array}{ll} 1, & \theta \leq \frac{25}{180}\pi \\ \frac{\frac{90}{180}\pi - \theta}{\frac{65}{180}\pi} - \frac{\left(\theta - \frac{25}{180}\pi\right)\left(\theta - \frac{90}{180}\pi\right)}{\frac{5000}{180}\pi}, & \frac{25}{180}\pi < \theta \leq \frac{90}{180}\pi \end{array} \right\}. \quad (2.11)$$

A_{SiCl_x} in equation 2.10 is equal to $0.353 \text{ eV}^{-0.5}$ according to the work of Tsuda et al. [54]. However, by using the latter value, we could not reproduce the etching rate measured by Nakazaki et al. [23]. In particular, the etching rate we calculated with the MC framework for ions with energy of 100 eV was about 4 times lower compared to the experimental value. Only if $f_{\text{SiCl}_x}(\theta)=1$ and no redeposition of etching products occurs, the value proposed by Tsuda et al. can reproduce the measured value of the etching rate. The value of A_{SiCl_x} given by Tsuda et al. is a “macroscopic” or phenomenological value, i.e. a value which can be extracted by an experiment which cannot quantify either the angle dependence of the etching yield for a surface morphology with nanoscale roughness or the redeposition of etching products. The “macroscopic” or phenomenological value captures the net effect of the ion bombardment taking into account all surface processes (including redeposition and angle dependence) but it is not suitable for a MC framework which treats separately each surface processes and not their net effect. For the framework, a “nanoscopic” value of A_{SiCl_x} is required to be determined. We adjusted this “nanoscopic” value of A_{SiCl_x} so that the calculated etching rate was fitted to the measured etching rate [23]. The adjusted value is included in Table 3.II in section 3.6.

The etching yield of physical sputtering depends on the ion energy and the angle of ion incidence, and reads [46, 54, 61]

$$EY_{\text{Si}} = A_{\text{Si}} \left(\sqrt{E_+} - \sqrt{E_{\text{th,Si}}} \right) f_{\text{Si}}(\theta) \quad (2.12)$$

The function f_{Si} expresses the angle dependence of the etching yield and reads [62]

$$f_{\text{Si}}(\theta) = \begin{cases} a_0, & \theta \leq \varphi_1 \\ b_0 + b_1\theta + b_2\theta^2 + b_3\theta^3, & \varphi_1 \leq \theta \leq \varphi_2 \\ 1 + c_2(\theta - \varphi_2)^2, & \theta \geq \varphi_2 \end{cases} \quad (2.13)$$

The constant parameters in equation 2.13 are

$$b_3 = \frac{a_0 - 1}{3\varphi_2\varphi_1(\varphi_1 - \varphi_2) - 3/2(\varphi_1 + \varphi_2)(\varphi_1^2 - \varphi_2^2) + (\varphi_1^3 - \varphi_2^3)},$$

$$b_2 = -(3/2)(\varphi_1 + \varphi_2)b_3,$$

$$b_1 = 3b_3\varphi_1\varphi_2,$$

$$b_0 = 1 - b_1\varphi_2 - b_2\varphi_2^2 - b_3\varphi_2^3, \text{ and}$$

$$c_2 = -\frac{1}{(\pi/2 - \varphi_2)^2}.$$

The parameters a_0 , φ_1 , and φ_2 (φ_1 , and φ_2 are in rad) define the exact form of the angle dependence (see figure 2.2); if their values are known, then parameters b_0 , b_1 , b_2 , b_3 and c_2 can be calculated. φ_2 is the angle corresponding to the maximum etching yield, a_0 is the ratio of the etching yield at normal incidence over the maximum etching yield. The space $[0, \varphi_1]$ defines the angle range that the etching yield is constant and equal to that at normal incidence. The values of a_0 , φ_1 , and φ_2 are coming from fitting of equation 2.13 to the curve of figure 2 in the work of Tsuda et al. [54] showing $f_{\text{Si}}(\theta)$: $a_0 = 1/2.1$, $\varphi_1 = (36/180)\pi$, and $\varphi_2 = (66/180)\pi$.

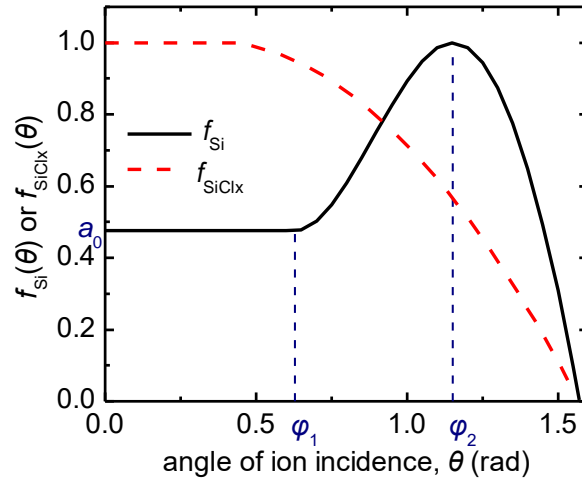


Figure 2.2 The functions $f_{\text{Si}}(\theta)$ (equation 2.13) and $f_{\text{SiCl}_x}(\theta)$ (equation 2.11) demonstrating the dependence of physical sputtering and ion-enhanced etching yield of Si on the angle of ion (Ar^+) incidence, θ . The parameters a_0 , φ_1 , and φ_2 of equation 2.13 are also noted.

$E_{\text{th,Si}}$ in equation 2.12 is the threshold energy for physical sputtering (in eV) and reads [46]

$$E_{\text{th,Si}} = 25.2 \left(\frac{M_t}{M_p} \right)^{-0.6} + 0.928 \frac{M_t}{M_p}. \quad (2.14)$$

A_{Si} in equation 2.12 is a coefficient (in $\text{eV}^{-0.5}$) which reads [46]

$$A_{\text{Si}} = 0.0054 \sqrt{Z_p Z_t \frac{M_t}{M_p M_t}} - 0.0198, \quad (2.15)$$

where M_p and Z_p and M_t and Z_t are the masses and atomic numbers of the projectile ions and the target atoms. In our case, the projectile ion is Cl^+ and the target atoms are Si, thus, $Z_p = 17$, $M_p = 35.4527$ amu, $Z_t = 14$, $M_p = 28.0855$ amu, and consequently $E_{\text{th,Si}} = 29.7$ eV and $A_{\text{Si}} = 0.0356$ $\text{eV}^{-0.5}$.

As in the case of A_{SiCl_x} (cf. the discussion above), the latter value is a “macroscopic” value. For the MC framework, a “nanoscopic” value of A_{Si} is required. We adjusted this “nanoscopic” value of A_{Si} so that the calculated etching yield was fitted to the “macroscopic” etching yield (see Eq. 2.12) for $f_{\text{Si}}(\theta)=1$. The adjusted value is included in Table 3.IV in section 3.7.

The sticking probability of Cl^+ on Si surface follows a cosine law (see figure 2.3); the reemission mechanism is specular reflection (angle of reemission is equal to the angle of incidence) and the energy of the reflected neutralized ion is considered equal to its energy before the impact. Ono and coworkers [54-56, 58] proposed a more detailed approach for the sticking probability, the direction and the energy of the reemitted (neutralized) ions based on calculations with the SRIM code [63]; the approach followed in this work is a good approximation of the behavior of the ions.

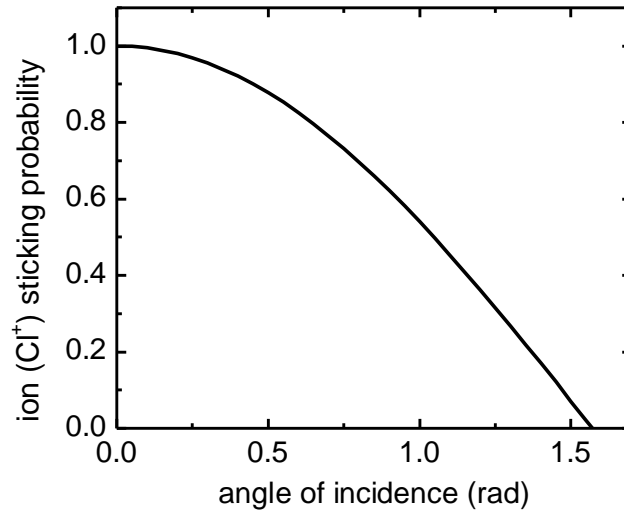


Figure 2.3 Cl⁺ sticking probability on SiCl_x(s) ($x=0,1,2,3$, and 4).

It has to be noticed that the etching yield adopted in this work (input to the code) gives the Si atoms removed per sticking ion. First, it is checked if the ion sticks on the surface. If the ion sticks, then a cell is removed or not based on the etching yield. The etching yield being used in the MC framework is per sticking ion and comes from the division of the etching yield per incident ion (see equations 2.10 and 2.12) with the sticking probability of ions.

Finally, the etch products can be redeposited on the Si surface (reaction 5 in Table 2.1) with a sticking probability, S_d . The etching products are assumed to be desorbed from the surface thermally following the cosine law [23, 54]. S_d is assumed equal to 0.05 in the work of Tsuda et al. [55]. However, in this work, this value was changed from 0 (no redeposition) to 1.0 and different values of A_{SiCl_x} were extracted.

In Figure 2.4, the energy dependence of the etching yields for ion-enhanced etching and physical sputtering (equations 2.10 and 2.12) are shown for $A_{\text{SiCl}_x} = 0.353 \text{ eV}^{-0.5}$ [54] and $A_{\text{Si}} = 0.0356 \text{ eV}^{-0.5}$ [46].

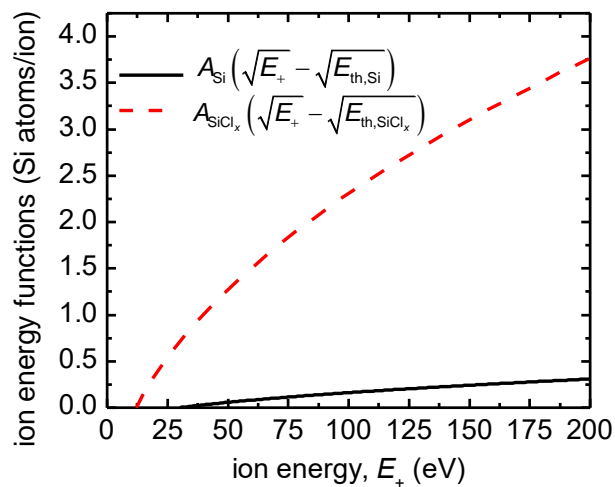


Figure 2.4 Ion energy functions of the etching yield expressions (from equations 2.10 and 2.12) for $A_{\text{SiCl}_x} = 0.353 \text{ eV}^{-0.5}$ [54] and $A_{\text{Si}} = 0.0356 \text{ eV}^{-0.5}$ [46].

2.3 Monte Carlo framework for the evolution of surface morphology

2.3.1 Basic concepts of the framework [19]

A modeling framework for surface morphology evolution in (2+1)d is exploited to apply the roughening mechanisms of Si surface under Cl_2 plasma. In the context of this framework, the etched film is represented by a lattice of cubic cells (see figure 2.5) and the solid on solid approximation [64] is considered. Particles with user defined angular distributions impinge on the cellular morphology. No particle-particle collisions are considered due to the high Knudsen number of the flow in the valleys of the surface morphology; the mean free path is large due to the low pressure conditions during plasma etching compared to the dimensions of valleys. The trajectory of each particle is calculated until sticking on a cell. The interaction of particles with the cells is defined by a) the sticking probability and b) the etching yield. Monte Carlo method is used to sample stochastic variables from probability distributions defining the initial position and direction of the particle, the etching yield, the reemission probability, and the direction of reemitted particles. More details for the simulation procedure are included in section 2.2.2. Statistical parameters of the surface morphology are extracted by a module for the characterization of the surface morphology (Section 2.2.3)

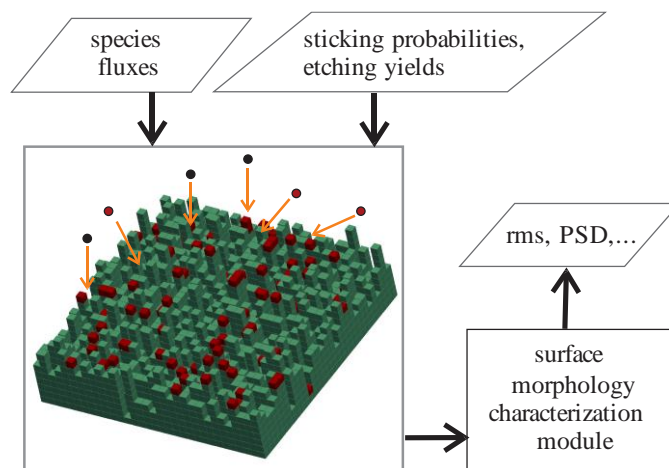


Figure 2.5 Schematic with the inputs and the outputs of the MC modeling framework

2.3.2 The simulation procedure

The simulation procedure requires the generation of a series of random numbers: For each decision a random number is generated. The steps of the procedure are the following:

a) A particle of ions (Cl^+) or reactive neutral species (Cl) is generated; the decision for the type of the particle is based on the fraction of each species in the arriving flux.

b) The initial position of the particle on a plane at a short distance (5 lattice units) from the higher point of the surface morphology is randomly chosen.

c) The initial direction of the particle is randomly chosen from the directions allowed by the direction distribution function of the particle (e.g. Gaussian for ions).

d) The particle moves on a straight line (no collisions in the gas phase due to the high Knudsen number) with discrete steps until its collision with the surface. The position and the cell of the collision are calculated. The type of the cell (substrate, i.e. Si in this work) as well as the chlorination level of the cell are identified.

e) Based on the sticking probability, the sticking or the reemission of the particle is decided. If the particle does not stick, the local slope of the surface is calculated and a reemission direction is chosen from the allowed ones by its reemission mechanism (e.g. diffuse reemission for neutral species).

Steps (d) and (e) are repeated until the particle sticks on the surface or escapes from the simulation domain. A particle escapes from the simulation when it crosses the plane of its “birth” [step (b)]; if the particle escapes, a new particle is generated [step (a)]. If the particle gets out of the domain from a different plane, it re-enters the domain from the opposite parallel plane: Periodic boundary conditions for the particle trajectories are considered.

f) If a particle of ions sticks on the surface, then etching or not is decided based on the etching yield. If the decision is etching, then the cell of the collision is removed from the lattice. Otherwise, a new particle is generated [step (a)]. If there are no cells below the added one, the added cell “slides” vertically until it meets one (solid on solid approximation).

The steps (a) to (f) are repeated for the total number of particles.

2.3.3 Surface morphology characterization

Besides the modeling framework, critical for the evaluation of a roughness mechanism is a module for the surface morphology characterization (see the flowchart in figure 2.5). The measures used to characterize the surface morphologies, i.e. the outputs of the simulations, refer to the surface roughness, the existence of dots on the surface, and the emergence of periodicity. In particular, root mean square (rms) roughness or surface width quantifies the vertical fluctuations of the surface morphology. The horizontal extent of the surface roughness is characterized by the correlation length, ξ ; it is a measure of the mean width of the surface features (e.g. dots). The skewness, which quantifies the asymmetry of the surface morphology, is used to identify the type of pattern on the surface: Positive skewness means that dots dominate on the surface morphology, while if skewness is negative, holes dominate [65]. The periodicity of a surface morphology is manifested by a peak in the power spectral density (PSD) [66, 67]. This does not mean that the surface morphology exhibits a perfect periodicity and only one wavelength. A dominating or characteristic wavelength exists. The 2d PSD is calculated and a circular average of the 2d PSD is extracted. Furthermore, parameter ω is defined to quantify the periodicity. ω is the ratio of the system correlation length, ζ [68, 69], over the period, λ . ζ is the inverse of the full width at half maximum of the PSD. The greater ω is, the stronger the periodicity is. Further information on the statistical parameters of surface morphology as well as formulas for their calculations can be found in ref. [69]. In this, work only the rms roughness of the evolving morphologies is presented

2.3.4 Time and space dimensions

The primary calculations with the Monte Carlo surface model show the evolution of the surface morphology in lattice units versus a normalized time variable, \hat{Q}_+ (see the definition below). The aim of the following paragraphs is the formulation of the required parameters and equations to assign real dimensions to the lattice unit and normalized time.

The lattice of the cellular morphology is coarse grained, i.e., it consists of super cells: Each super cell (SC) stands for a group of Si atoms of the substrate. All SCs have the same volume, V_{SC} , which can be approximated by the following equation

$$V_{SC} = d^3 = q_s / \rho_s, \quad (2.16)$$

where q_s is the number of atoms or molecules or monomers in the SC, ρ_s is the number density (monomer, molecules or atoms) of the substrate, and d is the length of the side of the cube of the SC.

The morphology evolution predicted by the modeling framework comes from the interaction of super particles with SCs. A super particle (SP) consists of a group of atoms or molecules or ions of the species joining the surface processes; a different type of SP is devised for each species. If the real etching yield of the substrate, i.e., the number of atoms or molecules or monomers removed per ion, is EY , then the etching yield of a SC of the substrate by a SP of ions is

$$EY_{SC} = EY \frac{q_+}{q_s}, \quad (2.17)$$

where q_+ is the number of ions in the SP of ions.

A constraint is that a SP cannot remove more than one SC; thus, the following inequality should hold

$$EY \frac{q_+}{q_s} \leq 1. \quad (2.18)$$

If EY_{max} is the maximum value of the etching yield in the conditions of the runs to be compared, then we choose

$$EY_{max} \frac{q_+}{q_s} = 1. \quad (2.19)$$

Combining equations 2.17 with 2.19 it comes that

$$EY_{SC} = \frac{EY}{EY_{max}}, \quad (2.20)$$

If \hat{Q}_+ is the number of SPs of ions arriving on the substrate over the number of SCs consisting a single layer of the substrate, and Γ_+ is the ion flux on the substrate, the etching time reads

$$t = \frac{\hat{Q}_+ q_+}{N^2 \Gamma_+ d^2}. \quad (2.21)$$

Γ_+ is coming from experimental measurements (or from calculations by a reactor scale model) and \hat{Q}_+ is a known independent variable of the surface model. By defining EY_{max} , ρ_s , and the desired discretization, i.e., d , we can assign absolute values to the etching time t .

Besides ions, a reactive neutral species arrives on the surface, the fraction of ions (not SP of ions) in the incoming flux is

$$x_+ = \frac{\hat{x}_+ q_+}{\hat{x}_+ q_+ + \hat{x}_N q_N} \quad (2.22)$$

where \hat{x}_+ and $\hat{x}_N (=1 - \hat{x}_+)$ are the fractions of SPs of ions and neutral species in the incoming flux and q_N is the number of neutral atoms (or molecules) in the SP of neutrals. Solving equation 2.22 for \hat{x}_+ , it comes that

$$\begin{aligned} x_+ &= \frac{\hat{x}_+ q_+}{\hat{x}_+ q_+ + (1 - \hat{x}_+) q_N} = \frac{\hat{x}_+ q_+}{\hat{x}_+ q_+ + q_N - \hat{x}_+ q_N} \quad \text{or} \\ (\hat{x}_+ q_+ + q_N - \hat{x}_+ q_N) x_+ - \hat{x}_+ q_+ &= 0 \quad \text{or} \\ \hat{x}_+ x_+ (q_+ - q_N) + q_N x_+ - \hat{x}_+ q_+ &= 0 \quad \text{or} \\ \hat{x}_+ [x_+ (q_+ - q_N) - q_+] &= -q_N x_+ \quad \text{or} \\ \hat{x}_+ &= \frac{-q_N x_+}{x_+ (q_+ - q_N) - q_+} \quad \text{or} \\ \hat{x}_+ &= \frac{q_N x_+}{q_+ - x_+ (q_+ - q_N)} \end{aligned} \quad (2.23)$$

Thus, if the value of q_N is defined, the value of \hat{x}_+ (and as a consequence of \hat{x}_N) is calculated by equation 2.23.

In case that the surface model includes the process of “neutralization” of an elementary surface (e.g. chlorination of the elementary surface) and the full “neutralization” of an atom of the substrate requires k_{\max} atoms of the neutral species (e.g. 4 atoms of Cl are required for the full chlorination of a Si atom), then the SP of neutral species required for the full “neutralization” of a SC is

$$\hat{k}_{\max} = k_{\max} \frac{q_S}{q_N}. \quad (2.24)$$

Thus, the level of “neutralization” is defined as the ratio of \hat{k} / \hat{k}_{\max} , where \hat{k} is the number of SPs of neutral species currently adsorbed on the SC.

In the case a reactive neutral species join the set of species arriving on the surface, \hat{Q}_+ is not the total number of SPs (over the number of SCs consisting a single layer of the substrate). The total number of SPs arriving on the surface, i.e. \hat{Q} , is related to \hat{Q}_+ with the following equation

$$\hat{Q}_+ = \hat{x}_+ \hat{Q}. \quad (2.25)$$

The combination of equations 2.21 with 2.25 reads

$$t = \frac{\hat{x}_+ \hat{Q} q_+}{N^2 \Gamma_+ d^2} \quad (2.26)$$

which gives the etching time as a function of \hat{Q} .

3. RESULTS

3.1 Introduction

The surface model (cf. Section 2.2) is implemented in the Monte Carlo framework for the evolution of the surface morphology (cf. Section 2.3) to predict the evolution of roughness developed on Si surfaces during Cl_2 plasma etching. The simulation results are compared to measurements of the etching rate and root mean square (rms) roughness by Nakazaki et al. [23]. The measurements of Nakazaki et al. are shown in figure 3.1: In particular, the etching rate was measured to increase with the ion energy (figure 3.1a), while a maximum at ~ 250 eV was measured for the rms roughness (figure 3.1b). The measurements were obtained in an inductively coupled plasma (ICP) reactor working at rf frequency (13.56 MHz). The power was $P_{\text{ICP}} = 450$ W. The pressure was 20 mTorr. The flow rate of Cl_2 was 5 – 50 sccm. The ion energy was 20 to 500 eV by changing the rf bias power from 0 to 200 W.

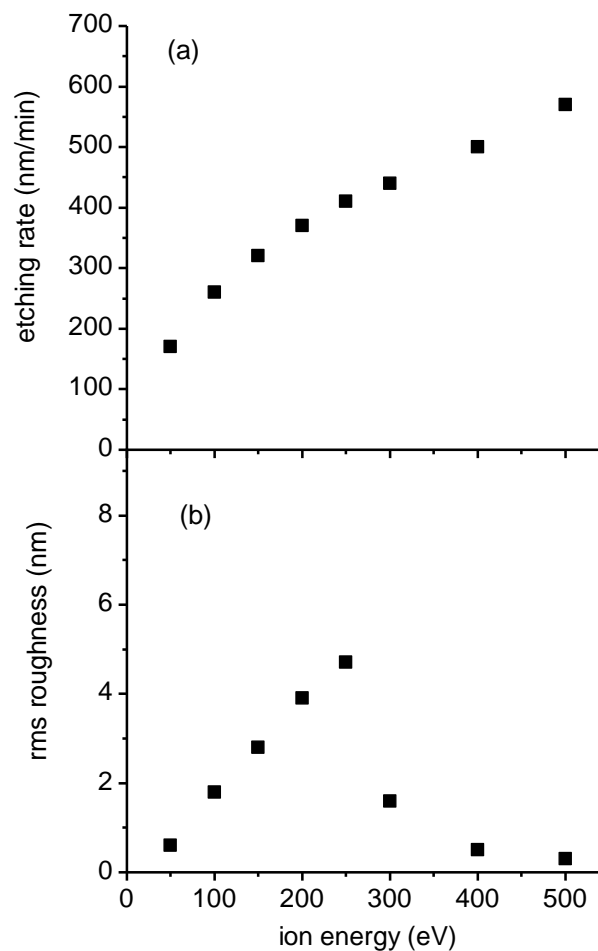


Figure 3.1 a) Etching rate and b) rms roughness of Si surfaces under Cl_2 plasma measured by Nakazaki et al. [23].

The dominant etching mechanism in plasma etching of Si substrates by Cl_2 plasmas is ion-enhanced etching. Thus, a critical parameter for the surface model is the ion-enhanced etching yield and in particular the coefficient A_{SiCl_x} of equation 2.10. According to the work of Tsuda et al. [54], A_{SiCl_x} is equal to $0.353 \text{ eV}^{-0.5}$. However, by using the latter value, we could not reproduce the etching rate measured by Nakazaki et al. [23]. In particular, the etching rate we calculated with the MC framework for ions with energy

of 100 eV was ~ 4 times lower compared to the experimental value. Only if there is no angle dependence of the ion-enhanced etching yield, i.e. $f_{\text{SiCl}_x}(\theta)=1$ in equation 2.10, and no redeposition of etching products occurs, the value proposed by Tsuda et al. can reproduce the measured value of the etching rate (see section 3.5).

However, although the exact function determining the dependence is not always accurately defined, angle dependence of the etching yield is a fact, and the redeposition is a phenomenon which cannot be directly measured. The origin of the value of A_{SiCl_x} is from a fitting to measurements and thus this value inherently entails an average effect of the angle of ion incidence and the redeposition. The fitting is usually based on beam experiments: The etching rate is measured for known flux and energy of ions and the etching yield is calculated by the division of the measured etching rate with the ion flux.

Due to the roughness developed on the etched surface, the ions meet different slopes on the same surface. Due to the roughness change, these slopes also change during the experiment. **Thus, the etching yield, and as a consequence A_{SiCl_x} , incorporates an average effect of the angle of ion incidence which varies in space and time during the experiment.**

The value of A_{SiCl_x} given by Tsuda et al. is a “macroscopic” or phenomenological value, i.e. a value extracted by an experiment which cannot quantify either the angle dependence of the etching yield for a surface morphology with nanoscale roughness and the redeposition of etching products. The “macroscopic” or phenomenological value captures the net effect of the ion bombardment taking into account all surface processes (including redeposition and angle dependence of etching) but it is not suitable for a MC framework which treats separately each surface process and not their net effect. For the framework, a “nanoscopic” value of A_{SiCl_x} is required to be determined.

In the following, we adjust this “nanoscopic” value of A_{SiCl_x} so that the calculated etching rate is fitted to the measured etching rate [23] (see Sections 3.5 and 3.6). Due to the fact that the redeposition cannot be directly measured, this adjustment is performed for different values of the sticking probability of the redeposited etching products, S_d (see Table 2.1) When $S_d=0$, no redeposition takes place, when $S_d=1$ the etching products are redeposited with a probability of 100%. The “nanoscopic” values of A_{SiCl_x} (for different values of S_d) are extracted for an ion energy equal to 100 eV; then using the values of A_{SiCl_x} and S_d we compare the model with the experimental results of Nakazaki et al. [23], referring to the etching rate and the rms roughness versus the ion energy (50 – 500 eV) (see Section 3.8). First of all, the effects of the dimensions of the surface and the unit cell of the MC framework on the calculated etching rate and rms roughness are investigated (see Sections 3.3 and 3.4)

3.2 Case study

All values used for the inputs of the models are typical for inductively coupled plasma (ICP) and electron cyclotron resonance (ECR) discharges [56]. The conditions (values of inputs) are [56]: Ion energy, $E_+ = 100$ eV, standard deviation of angular distribution of ions, $\sigma = 0.05$ rad, gas temperature, $T_g = 500$ K. The etched surface is plane n-type Si(100) surface with atomic density equal to $5 \times 10^{22} \text{ cm}^{-3}$. The dopant concentration is $N_e = 1.01 \times 10^{18} \text{ cm}^{-3}$ and the surface temperature is $T_s = 320$ K. The ion (Cl^+) flux, Γ_+ , is

$10^{20} \text{ m}^{-2}\text{s}^{-1}$ and the ratio of neutral (Cl) to ion (Cl⁺) flux is 100. The angle of the main direction of the ions arriving on the surface with the normal to the surface is 0° .

Table 3.I The values of the parameters used for the runs. The total etching time is 120 s for all cases. A_{SiCl_x} and A_{Si} are the parameters defining the ion-enhanced and physical sputtering yield (see equations 2.10 and 2.12), a_{chem} is the coefficient of pure chemical reaction of a saturated (with Cl) Si surface, x_+ is the fraction of ions in the arriving flux, S_d is the sticking probability of the etching products, E_+ is the ion energy, $f_{\text{SiCl}_x}(\theta)$ is the function defining the angle dependence of the ion-enhanced etching yield (see equation 2.11).

| case | A_{SiCl_x} (eV ^{-0.5}) | A_{Si} (eV ^{-0.5}) | a_{chem} | x_+ | S_d | E_+ (eV) | $f_{\text{SiCl}_x}(\theta)$ | Surface dimension (nm ²) | Cell dimension (nm ³) | Number of runs |
|------|--|--|-------------------|--------|----------|---------------|-----------------------------|--|---|----------------------|
| 0001 | 1.3061 | 0 | 0 | 1* | 1 | 100 | Eq. 2.11 | 512x512 | 1 | 6 |
| 0002 | 1.3061 | 0 | 0 | 1* | 1 | 100 | Eq. 2.11 | 256x256 | 1 | 6 |
| 0003 | 1.3061 | 0 | 0 | 1* | 1 | 100 | Eq. 2.11 | 128x128 | 1 | 6 |
| 0004 | 1.3061 | 0 | 0 | 1* | 1 | 100 | Eq. 2.11 | 64x64 | 1 | 6 |
| 0005 | 1.3061 | 0 | 0 | 1 | 1 | 100 | Eq. 2.11 | 128x128 | 0.585 ³ | 6 |
| 0006 | 1.3061 | 0 | 0 | 1 | 1 | 100 | Eq. 2.11 | 128x128 | 0.271 ³ | 6 |
| 0007 | 0.353 | 0.0356 | 0.0009 | 0.0099 | 0.05 | 100 | Eq. 2.11 | 50x50 | 0.271 ³ | 3 |
| 0008 | 0.353 | 0.0356 | 0.0009 | 0.0099 | 0 | 100 | 1 | 50x50 | 0.271 ³ | 3 |
| 0009 | 0.3354 – 0.7237 | 0 | 0 | 1 | 0 – 1 | 100 | 1 | 64x64 | 1 | 1 per S_d value |
| 0010 | 1.3061 – 2.0121 | 0 | 0 | 1 | 0 – 1 | 100 | Eq. 2.11 | 64x64 | 1 | 1 per S_d value |
| 0011 | 1.3061 – 1.9768 | 0 | 0.0009 | 0.0099 | 0 – 1 | 100 | Eq. 2.11 | 64x64 | 1 | 1 per S_d value |
| 0012 | 1.3061 – 1.9768 | 0.0178 – 0.0338 | 0.0009 | 0.0099 | 0 – 1 | 100 | Eq. 2.11 | 64x64 | 1 | 1 per S_d value |
| 0013 | 0 | 0.0178 – 0.0338 | 0 | 1 | 0 – 1 | 100 | - | 64x64 | 1 | 1 per S_d value |
| 0014 | 1.9768 | 0 | 0 | 1 | 0.05 | 50 | Eq. 2.11 | 128x128 | 0.271 ³ | 5 |
| 0015 | 1.9768 | 0 | 0 | 1 | 0.05 | 100 | Eq. 2.11 | 128x128 | 0.271 ³ | 5 |
| 0016 | 1.9768 | 0 | 0 | 1 | 0.05 | 150 | Eq. 2.11 | 128x128 | 0.271 ³ | 5 |
| 0017 | 1.9768 | 0 | 0 | 1 | 0.05 | 200 | Eq. 2.11 | 128x128 | 0.271 ³ | 5 |
| 0018 | 1.9768 | 0 | 0 | 1 | 0.05 | 250 | Eq. 2.11 | 128x128 | 0.271 ³ | 5 |
| 0019 | 1.9768 | 0 | 0 | 1 | 0.05 | 300 | Eq. 2.11 | 128x128 | 0.271 ³ | 5 |
| 0020 | 1.9768 | 0 | 0 | 1 | 0.05 | 400 | Eq. 2.11 | 128x128 | 0.271 ³ | 5 |
| 0021 | 1.9768 | 0 | 0 | 1 | 0.05 | 500 | Eq. 2.11 | 128x128 | 0.271 ³ | 5 |
| 0022 | 1.9768 | 0 | 0 | 1 | 1 | 50 | Eq. 2.11 | 128x128 | 0.271 ³ | 5 |
| 0023 | 1.9768 | 0 | 0 | 1 | 1 | 100 | Eq. 2.11 | 128x128 | 0.271 ³ | 5 |
| 0024 | 1.9768 | 0 | 0 | 1 | 1 | 150 | Eq. 2.11 | 128x128 | 0.271 ³ | 5 |
| 0025 | 1.9768 | 0 | 0 | 1 | 1 | 200 | Eq. 2.11 | 128x128 | 0.271 ³ | 5 |
| 0026 | 1.9768 | 0 | 0 | 1 | 1 | 250 | Eq. 2.11 | 128x128 | 0.271 ³ | 5 |
| 0027 | 1.9768 | 0 | 0 | 1 | 1 | 300 | Eq. 2.11 | 128x128 | 0.271 ³ | 5 |
| 0028 | 1.9768 | 0 | 0 | 1 | 1 | 400 | Eq. 2.11 | 128x128 | 0.271 ³ | 5 |
| 0029 | 1.9768 | 0 | 0 | 1 | 1 | 500 | Eq. 2.11 | 128x128 | 0.271 ³ | 5 |

3.3 The effect of the dimensions of the surface on the calculated etching rate and rms roughness

We examine the effect of the surface dimension on the etching rate and the rms roughness. Runs with different dimensions of the surface, i.e. 512x512, 256x256, 128x128, and 64x64 nm², are performed. The dimension of the unit cell is kept constant and equal to 1 nm³. The conditions and the parameters used for the cases (0001 – 0004) are described in Table 3.I. In all cases, pure chemical etching is neglected. It is also considered that the surface is fully chlorinated which can be justified by the high ratio of flux of Cl over the flux of Cl⁺ (100); thus, there is no need to consider the

transport of Cl atoms. Both assumptions are made to accelerate the runs. The evolution of the etching rate and the rms roughness versus time are shown in Figures 3.2a and 3.2b respectively.

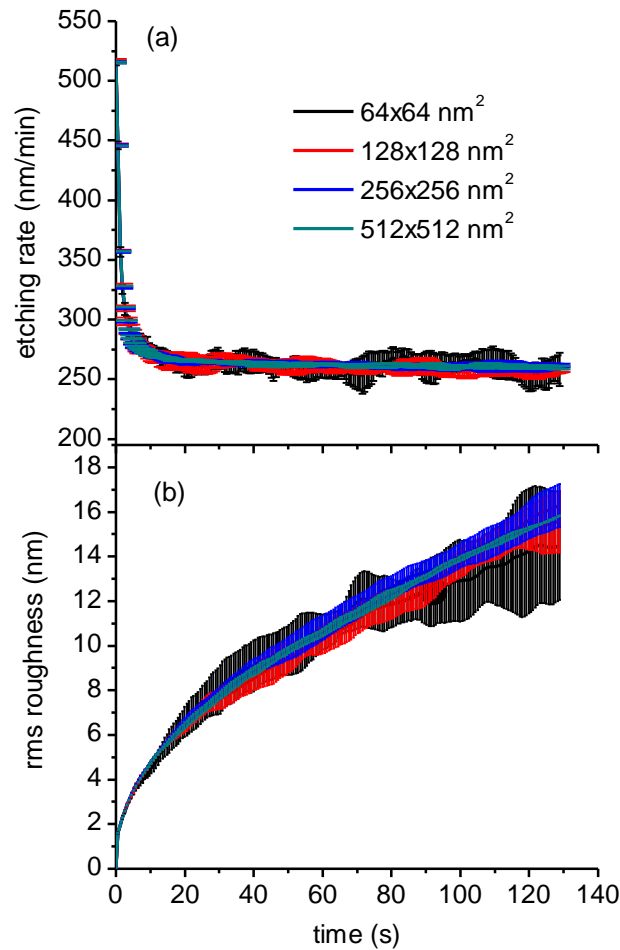


Figure 3.2. a) The etching rate (average value of 6 runs per case) and **b)** the rms roughness (average value of 6 runs per case) versus time for surfaces with different dimensions, i.e. 512×512 nm², 256×256 nm², 128×128 nm², and 64×64 nm². The results correspond to cases 0001 to 0004 of Table 3.I.

The results show that both the etching rate and the rms are not affected by the dimensions of the surface. The values obtained are similar for all the surface dimensions. It is also observed that the standard deviation of the etching rate and mainly the rms roughness increases as the surface area decreases. In order to decrease the execution time and reduce the error bars, it is decided to use a surface of 128×128 nm² for the rest of the runs.

3.4 The effect of the dimensions of the unit cell on the calculated etching rate and rms roughness

In this paragraph the effect of the cell dimension is investigated. Runs with different dimensions of the unit cell, i.e. 1×1×1 nm³, 0.585×0.585×0.585 nm³, and 0.271×0.271×0.271 nm³ are performed. When the volume of the unit cell is 1 nm³, unit cell consists of 50 Si atoms, when the volume of the cell is 0.585³ nm³, the unit cell contains 10 Si atoms, and in the case that the volume of the unit cell is 0.271³ nm³, the

unit cell is no longer considered 'super particle' as it contains only one Si atom. The dimension of the surface is kept constant and equal to $128 \times 128 \text{ nm}^2$. The aim is to investigate the effect of the dimensions of the unit cell on the etching rate and rms roughness. The conditions and the parameters used for the runs are described in Table 3.1 (cases 0003, 0005, and 0006). As in Section 3.3, for all cases, pure chemical etching is neglected. It is also considered that the surface is fully chlorinated which can be justified by the high ratio of flux of Cl over the flux of Cl^+ (100); thus, there is no need to consider the transport of Cl atoms. Both assumptions are made to accelerate the runs.

As shown in Figure 3.3a, not important differences are observed on the etching rate with the change of the unit cell volume. Regarding rms roughness though, the effect of the unit cell volume is remarkable (see Figure 3.3b): For example, at 120 s, it is $\sim 15 \text{ nm}$ for volume equal to 1 nm^3 , it is $\sim 12 \text{ nm}$ for volume equal to 0.585 nm^3 , and it is $\sim 7 \text{ nm}$ for volume equal to 0.271^3 nm^3 . This suggests that we cannot use coarse graining. It is decided to use the minimum dimension of the unit cell, i.e. 0.271^3 nm^3 , which includes only one Si atom.

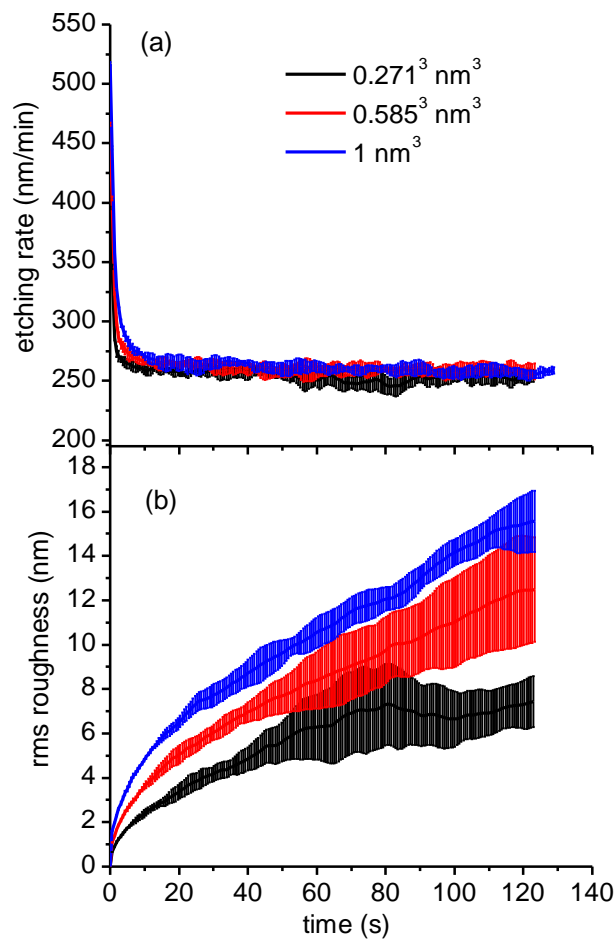


Figure 3.3. a) The etching rate (average value of 6 runs) and b) the rms roughness (average value of 6 runs) for an $128 \times 128 \text{ nm}^2$ surface and unit cell dimensions of 1 nm^3 , 0.585^3 nm^3 and 0.271^3 nm^3 . The results correspond to cases 0003, 0005, and 0006 of Table 3.1.

3.5 First comparison of the calculated etching rate with measurements

The first comparison of the model results with the measurements is made at an ion energy of 100 eV where the etching rate was measured [60] $\sim 260 \text{ nm/min}$ (at 120 s), respectively. When we use the values proposed by Tsuda et al. [54, 56] in the surface

model (see case 0007 in Table 3.I), the etching rate is calculated ~ 60 nm/min (see Figure 3.4), i.e. four times smaller than the experimental value.

In order to investigate the origin of the difference between the model and the experimental results, the first step was to check the effect of the model assumptions on the results. **After some trial runs, it was found that, if the angle dependence of the ion enhanced etching yield (see Equation 2.10) and the product redeposition were both neglected (case 0008 in Table 3.II), the etching rate was calculated ~ 270 nm/min (see Figure 3.4), i.e. very close to the experimental results.**

If we accept that the angle dependence of the etching yield is a fact (and thus we cannot assume that $f_{\text{SiCl}_x}(\theta)=1$, and given that the dominant mechanism of Si etching by Cl_2 plasma is ion-enhanced etching, a critical parameter for the value of the calculated etching rate is A_{SiCl_x} of equation 2.10. As discussed in sections 2.2.2 and 3.1, a “nanoscopic” value of the A_{SiCl_x} is required for the MC framework. The procedure we followed to extract this “nanoscopic” value is described in section 3.6.

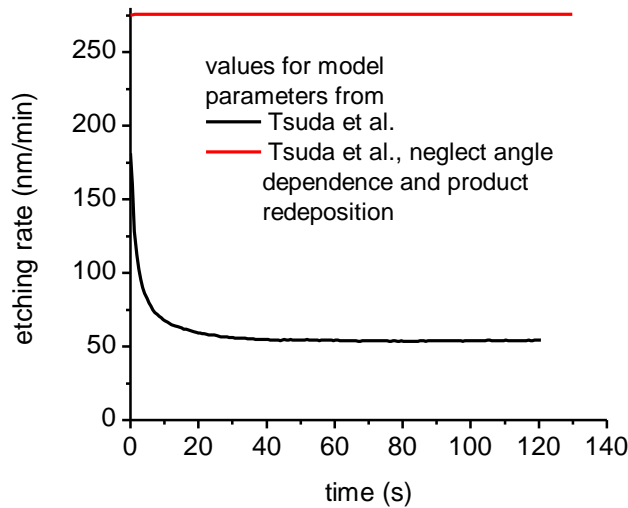


Figure 3.4. The etching rate (average value of 3 runs) for an 128×128 nm² surface and unit cell dimensions of 0.271 nm³. The results for two cases (cases 0007 and 0008 of Table 3.I) are shown. In the first case, the parameters of the surface model are taken from Tsuda et al. [54, 56] are used. In the second case, no angle dependence of the etching yield and no redeposition of etching products are considered, i.e. $f_{\text{SiCl}_x}(\theta)=1$ (see equation 2.10) and $S_d = 0$.

3.6 Extraction of “nanoscopic” values of the parameter defining the ion-enhanced etching yield

The “nanoscopic” value of A_{SiCl_x} (see equation 2.10) is extracted by a trial and error procedure: Several values of A_{SiCl_x} are checked until the calculated etching rate at an ion energy equal to 100 eV is close to the measured value of the etching rate (~ 270 nm/min). The uncertainty of the value of the sticking probability of the redeposited products, S_d ($S_d=0$ means no redeposition of etching products, $S_d=1$ means that all molecules of etching products stick with 100% probability if they meet the etched surface after their production and emission), manifests the requirement for a parametric analysis: The “nanoscopic” value of A_{SiCl_x} reproducing the experimentally measured etching rate will be calculated by the trial and error procedure for several values of S_d

from 0 to 1. The “nanoscopic” values of A_{SiCl_x} are shown in Table 3.II. We performed a series of runs, starting from a simple case where the runs are really fast. We then used the calculated values of A_{SiCl_x} as initial estimations for more complex cases.

In the first series of runs (case 0009 in Table 3.I, first row of Table 3.II) we consider only ion-enhanced etching. Physical sputtering and pure chemical etching are not taken into account due to their small contribution to the etching rate. The surface is considered fully chlorinated surface given that the ratio of Cl to Cl⁺ fluxes is 100. Angle dependence of the ion-enhanced etching yield was neglected for this case.

In the second series of runs (case 0010 in Table 3.I, second row of Table 3.II), the conditions are the same as in case 0009 except that the angle dependence of the ion-enhanced etching yield is taken into account. Comparing the second with the first row of Table 3.II (case 0010 with 0009), it is obvious that the angle dependence increases the “nanoscopic” value of A_{SiCl_x} .

In the third series of runs (case 0011 in Table 3.I, third row of Table 3.II), the conditions are the same as in case 0010 except that chemical etching is taken into account. The surface is still considered fully chlorinated. Comparing the second with the third row of Table 3.II (case 0011 with 0010), it can be concluded that the values of A_{SiCl_x} are not noticeably altered with the addition of neutrals and the activation of chemical etching mechanism.

In the fourth series of runs (case 0012 in Table 3.I, fourth row in Table 3.II), the conditions are the same as in case 0011 except that the surface is not fully chlorinated; the chlorination level is defined by the Cl atoms arriving and sticking on the etched surface. As a consequence, physical sputtering is also activated. In this case, the full model is used. By comparing the fourth with the third row of Table 3.II (case 0012 with 001), it can be concluded that the effect of physical sputtering on the “nanoscopic” value of A_{SiCl_x} and on the calculated etching rate is indeed negligible. The calculations show that the surface is fully chlorinated.

Table 3.II The “nanoscopic” values of A_{SiCl_x} (in eV^{-0.5}) and S_d reproducing the experimental value of the etching rate for an ion energy equal to 100 eV (~260 nm/min) and for different values of S_d . The value proposed by Tsuda et al. [56] is 0.353 eV^{-0.5}.

| case / $S_d \rightarrow$ | 0.0 | 0.001 | 0.005 | 0.01 | 0.05 | 0.1 | 0.2 | 0.5 | 1.0 |
|--------------------------|--------|--------|--------|--------|--------|--------|--------|--------|--------|
| 0009 | 0.3354 | 0.4766 | 0.5648 | 0.6001 | 0.6354 | 0.6354 | 0.6707 | 0.6884 | 0.7237 |
| 0010 | 1.3061 | 1.6238 | 2.0121 | 1.9768 | 1.9768 | 1.8356 | 1.6944 | 1.4197 | 1.3061 |
| 0011 | | 1.6238 | 1.9415 | 1.9768 | 1.9768 | 1.8356 | 1.6591 | 1.4197 | 1.3061 |
| 0012 | | | 1.9415 | 1.9768 | 1.9768 | 1.8356 | 1.6591 | 1.4197 | 1.3061 |

The conclusions from the parametric analysis through the trial and error procedure described above are summarized below:

- The angle dependence of the ion-enhanced etching yield as well as the redeposition of etching products strongly affect the “nanoscopic” value of A_{SiCl_x} (coefficient of the ion-enhanced etching yield, equation 2.10).
- Chemical etching and physical sputtering have a negligible effect on the “nanoscopic” value of A_{SiCl_x} (coefficient of the ion-enhanced etching yield, equation 2.10) and on the etching rate.
- The calculations show that an assumption of a fully chlorinated surface is valid.

Thus, in the rest of the calculations presented in this work, we consider that the surface is fully chlorinated and the only etching mechanism is ion-enhanced etching. These assumptions allow for major acceleration of the calculations with the MC framework: Indeed, we avoid the computational cost of calculating the transport of Cl atoms which 100 times more than the ions arriving on the surface.

In Table 3.II, and in particular in the third row (case 0010) a series of “nanoscopic” values of A_{SiCl_x} are shown; but **what is the “right” one?** Or better how can we chose for the value of S_d ? In order to choose the value of S_d , we use the second measurement, i.e. the rms roughness of the etched surface. After reproducing a first order parameter of etching, namely the etching rate, the next step is to reproduce a second order parameter of etching, namely the rms roughness.

The values of rms roughness calculated when considering the “nanoscopic” values of A_{SiCl_x} and S_d from Table 3.II are shown in Table 3.III. It has to be noticed that the statistical error in the values of Table 3.III is high due to the small surface dimensions ($64 \times 64 \text{ nm}^2$), and a consequence of the small number of incident particles, and the small number of runs (only 1). Nevertheless, by observing the values in Table 3.III, it can be concluded that

- The angle dependence of the etching yield increases rms roughness.
- The increase of S_d decreases rms roughness
- The addition of chemical etching (cases 0011 and 0012) does not decrease rms roughness; this is not a safe conclusion due to the reason mentioned above (small number of incident particles and only 1 run)

Table 3.III The values of rms in nm for the “nanoscopic” values of A_{SiCl_x} and S_d from Table 3.II.

| case / $S_d \rightarrow$ | 0.0 | 0.001 | 0.005 | 0.01 | 0.05 | 0.1 | 0.2 | 0.5 | 1.0 |
|--------------------------|------|-------|-------|------|------|------|------|------|------|
| 0009 | 86.4 | 37.9 | 26.3 | 22.0 | 10.8 | 10.8 | 9.4 | 5.4 | 3.8 |
| 0010 | 98.1 | 56.2 | 42.1 | 35.0 | 32.9 | 32.9 | 32.4 | 17.0 | 8.9 |
| 0011 | | 54.3 | 38.2 | 36.5 | 28.1 | 31.0 | 28.3 | 16.2 | 8.9 |
| 0012 | | | | | 31.9 | 32.5 | 28.0 | 21.8 | 15.6 |

3.7 Extraction of “nanoscopic” values of the parameter defining the physical sputtering yield

A “nanoscopic” value is required not only for A_{SiCl_x} but also for A_{Si} . The origin of the value of A_{Si} met in published reports is “macroscopic”, i.e. it coming from a fitting to macroscopic measurements of the sputtering rate. Thus, this value inherently entails an average effect of the angle of ion incidence and the redeposition. The “nanoscopic” value of A_{Si} , which is suitable for a MC framework is extracted by fitting of the calculated etching rate at an ion energy of 100 eV to the value $0.0356(\sqrt{100} - \sqrt{29.7})10^{20} / (5 \times 10^{28}) = 19.4 \text{ nm/min}$. The latter value is coming by the “macroscopic” sputtering rate, i.e. by multiplying the sputtering yield (see Equation 2.12) with the ion flux for ions (see section 3.2) with energy of 100 eV and by dividing with the Si atom density. In the latter calculation, it has been considered that the ion meets a perfectly flat Si surface.

The “nanoscopic” values of A_{Si} are shown in Table 3.IV. Although in the cases studied physical sputtering is negligible compared to ion-enhanced etching, the “nanoscopic” values of A_{Si} may be very useful in cases where the ratio of Cl flux to Cl^+ flux is lower.

Table 3.IV The “nanoscopic” values of A_{Si} reproducing the “macroscopic” value of the physical sputtering rate (19.4 nm/min, ions at 100 eV with a flux of $10^{20} \text{ m}^{-2}\text{s}^{-1}$)

| case / $S_d \rightarrow$ | 0.0 | 0.001 | 0.005 | 0.01 | 0.02 | 0.1 | 0.2 | 0.5 | 1.0 |
|--------------------------|--------|--------|--------|--------|--------|--------|--------|--------|--------|
| 0013 | 0.0178 | 0.0214 | 0.0249 | 0.0249 | 0.0285 | 0.0285 | 0.0285 | 0.3204 | 0.0338 |

3.8 Comparison of model results with measurements of etching rate and rms versus the ion energy

The extraction of “nanoscopic” values of A_{SiCl_x} (and A_{Si}), as described in the sections 3.6 and 3.7, was performed at an ion energy equal to 100 eV. **But do these “nanoscopic” values predict the behavior of etching rate and rms roughness for other values of ion energy?** The answer is included in figure 3.5 where the simulation results are shown versus the ion energy. Two values of S_d (sticking probability of etching products) are used, i.e. 0.05 and 1. All runs included in figure 3.5 are described by cases 0014-0021 ($S_d=0.05$) and 0022-0028 ($S_d=1$) in Table 3.I. In figure 3.5, the measured [23] etching rate and rms roughness are also shown.

The MC modeling framework reproduces well the experimentally measured dependence of the etching rate on the ion energy (see figure 3.5a) for both values of S_d (0.05 and 1). Greater deviations are observed at greater ion energies, i.e. above 350 eV. Regarding the rms roughness (figure 3.5b), although the absolute values are overestimated, the behavior of rms roughness versus ion energy is captured by the MC modeling framework for the case $S_d=1$. It is interesting that the framework captures the existence of a maximum of rms roughness versus the ion energy. The maximum of the rms roughness is at ~300 eV for the simulation results and at ~250 eV for the measurements. When $S_d=0$, the calculated rms values are much greater compared to the measured values. The calculated values are getting lower when $S_d=1$, i.e. when the redeposition of the etching products is more intense. The redeposition favors lower values for rms. When redeposition is less intense, there is no maximum or saturation of the rms with the ion energy (see figure 3.5b, $S_d=0$).

The potential origins of the deviations between the simulation results and the experimental data are the following. **First, regarding the overestimation of the etching rate at high ion energies by the MC modeling framework**, the assumption of a fully chlorinated surface may not be valid at high ion energies; if the chlorination level of the surface (x in equation 2.10) decreases with the ion energy, the etching rate will also decrease. Additionally, the composition of the flux arriving on the surface may also change as the ion energy increases. The production rate of etching products increases with the ion energy and these etching products join the plasma reactions and may alter the composition of ions arriving on the surface. Tsuda et al. [56] reported that the fraction of heavy (light) ions, e.g. $SiCl_x^+$ (Cl^+), on the arriving flux increases (decreases) with the ion energy. The ion-enhanced etching yield of Si by $SiCl_x^+$ may be lower compared to the ion-enhanced yield of Si by Cl^+ .

Second, regarding the overestimation of the rms roughness by the MC modeling framework, there may be an underestimation of the sticking probability of ions on the surface. The reduction of the ion reflection is expected to decrease the rms roughness; ion reflection is a mechanism which enhances rms roughness. Additionally, given that

the sticking probability of ions depends on the angle of ion incidence (see figure 2.3), ion reflection may be also reduced by changing the method for the calculation of the local slope of the surface. In the MC modeling framework, the local slope of the surface at an impact point (point where an ion arrives) is calculated by exploiting the values of the first neighbors of the impact point. In particular, the local surface slope is calculated by the derivative of the following function describing the surface

$$z(x, y) = \sum_{j=1}^N z_j \varphi^j(x, y) \quad (3.1)$$

where z_j are the z coordinates of the surface on the nodes of the grid and φ^j are **linear (for the calculations in this work)** basis functions. The use of basis functions with a greater order would decrease the local slope and thus increase the sticking probability of the ions (cf. figure 2.3). The local slope has been calculated in previous works by taking into account 4 adjacent neighbors [42] and by taking into account 125 neighbors [54]. Regardless of the available options for the calculation of the local slope, the question remains. **The right choice requires a new study to investigate the notion of local slope in MC calculations.**

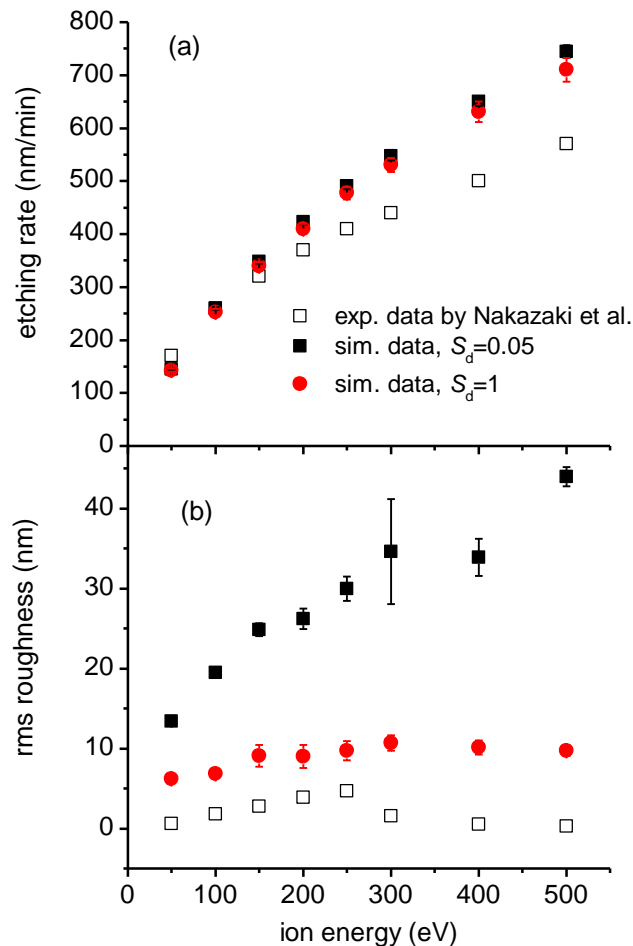


Figure 3.5 a) The etching rate and b) the rms roughness vs the ion energy as obtained from our simulation and the measurements of Nakazaki et al. [23]. The simulation results refer to cases 0014 to 0029: Two values of S_d are considered: $S_d=0.05$ and $S_d=1$. The error bars are coming from the standard deviations of the runs of each case.

4. CONCLUSIONS

A surface model for Si etching by Cl_2 plasma was developed and it was coupled with a Monte Carlo modeling framework to predict the etching rate and the rms roughness of Si surfaces. The surface model took into account ion-enhanced, physical sputtering, and pure chemical etching mechanisms; however, under the conditions of the calculations, ion-enhanced etching was dominant.

When the values of the surface model parameters were taken from the literature, the etching rate calculated by the Monte Carlo framework was 4 times lower compared to measurements. In particular, the comparison showed that the values of the physical parameters defining the etching yield, mainly for ion-enhanced etching but also for physical sputtering, are not suitable for use in Monte Carlo frameworks. The origin is that these values are usually coming from fitting to measurements and thus they inherently entail an average effect of the angle of ion incidence. The fitting is usually based on beam experiments: The etching rate is measured for known flux and energy of ions and the etching yield is calculated by the division of the measured etching rate with the ion flux. Due to the roughness developed on the etched surface, the ions meet different slopes on the same surface. Due to the roughness change these slopes also change during the experiment. Thus, the etching yield incorporates an average effect of the angle of ion incidence which varies in space and time during the experiment. This is the “macroscopic” etching yield. The “macroscopic” or phenomenological value captures the net effect of the ion bombardment taking into account all surface processes (including redeposition and angle dependence of etching) but it is not suitable for a Monte Carlo framework which treats separately each surface process and not their net effect.

For a Monte Carlo framework, the “nanoscopic” etching yield is required. This “nanoscopic” etching yield should be suitable to reproduce the “macroscopic” etching yield and rate. This is the procedure followed in this work: The “nanoscopic” etching yield of the dominant etching mechanism, namely ion-enhanced etching, was extracted by fitting the calculated etching rate to available measurements. This procedure was performed for one value of the ion energy (100 eV), and then the results of the modeling framework were compared to measurements of etching rate and rms roughness for different values of the ion energy (50 to 500 eV).

The Monte Carlo framework reproduced well the experimentally measured dependence of the etching rate on the ion energy. The etching rate was overestimated at ion energies greater than 350 eV. This overestimation may be due to the assumption of a fully chlorinated surface which may not be valid at high ion energies; if the chlorination level of the surface decreases with the ion energy, the etching rate will also decrease. Additionally, the composition of the flux arriving on the surface may also change as the ion energy increases; the fraction of heavy (light) ions, e.g. SiCl_x^+ (Cl^+), on the arriving flux increases (decreases) with the ion energy. The ion-enhanced etching yield of Si by SiCl_x^+ may be lower compared to the ion-enhanced yield of Si by Cl^+ .

Regarding the rms roughness, although the absolute values are overestimated, the behavior of rms roughness versus ion energy is captured when the redeposition of the etching products is intense. The origin of the overestimation, may be due to an underestimation of the sticking probability of ions on the surface. The reduction of the ion reflection is expected to decrease the rms roughness; ion reflection is a mechanism which enhances rms roughness. Additionally, given that the sticking probability of ions depends on the angle of ion incidence, ion reflection may be also reduced by changing the method for the calculation of the local slope of the surface. In

the Monte Carlo modeling framework, the local slope of the surface at an impact point (point where an ion arrives) is calculated by exploiting the values of the first neighbors of the impact point. The use of more neighbors in the calculation of the local slope would effectively decrease the local slope and thus increase the sticking probability of the ions.

Besides the comparison with measurements, the simulations with the Monte Carlo framework showed that coarse graining affected the value of the rms value being calculated, thus it was avoided.

Regarding the future works, given that the local slope is critical for both ion reflection and the ion-enhanced etching yield, a new investigation for right treatment of local slope will be a useful extension of the present study. Additionally, a study on the origin of the angle dependence of the etching yield and the means to incorporate this dependence in a Monte Carlo framework will be very interesting. Questions such as “what is the scale that the angle dependence of the etching yield is valid” will be investigated. The current study also pinpointed the importance of a study on the reflection (reemission) mechanism of Cl^+ ions on Si surfaces. Finally, the surface model and the Monte Carlo modeling framework can be integrated in a multiscale modeling framework [62] to take into account the change of the ion composition of the arriving flux.

REFERENCES

- [1] W. Guo and H. H. Sawin, "Review of profile and roughening simulation in microelectronics plasma etching," *Journal Of Physics D-Applied Physics*, vol. 42, no. 19, p. 194014, 2009.
- [2] K. Patel, T. J. K. Liu, and C. J. Spanos, "Gate Line Edge Roughness Model for Estimation of FinFET Performance Variability," *IEEE Transactions on Electron Devices*, vol. 56, no. 12, pp. 3055-3063, 2009.
- [3] K. Eriguchi, Y. Takao, and K. Ono, "Modeling of plasma-induced damage and its impacts on parameter variations in advanced electronic devices," *Journal of Vacuum Science & Technology A: Vacuum, Surfaces, and Films*, vol. 29, no. 4, p. 041303, 2011.
- [4] N. Tayebi and A. A. Polycarpou, "Reducing the effects of adhesion and friction in microelectromechanical systems (MEMSs) through surface roughening: Comparison between theory and experiments," *Journal of Applied Physics*, Journal Article vol. 98, no. 073528, pp. 1-13, 2005.
- [5] K. Sugano and O. Tabata, "Reduction of surface roughness and aperture size effect for etching of Si with XeF₂," *Journal of Micromechanics and Microengineering*, vol. 12, no. 6, p. 911, 2002.
- [6] N. Vourdas, A. Tserepi, and E. Gogolides, "Nanotextured super-hydrophobic transparent poly(methyl methacrylate) surfaces using high-density plasma processing," *Nanotechnology*, vol. 18, no. 12, p. 125304, 2007.
- [7] K. Ellinas, A. Tserepi, and E. Gogolides, "From Superamphiphobic to Amphiphilic Polymeric Surfaces with Ordered Hierarchical Roughness Fabricated with Colloidal Lithography and Plasma Nanotexturing," *Langmuir*, vol. 27, no. 7, pp. 3960-3969, 2011.
- [8] E. Gogolides *et al.*, "Controlling roughness: from etching to nanotexturing and plasma-directed organization on organic and inorganic materials," *Journal Of Physics D: Applied Physics*, vol. 44, no. 17, p. 174021, 2011.
- [9] K. Tsougeni, A. Tserepi, V. Constantoudis, E. Gogolides, P. S. Petrou, and S. E. Kakabakos, "Plasma Nanotextured PMMA Surfaces for Protein Arrays: Increased Protein Binding and Enhanced Detection Sensitivity," *Langmuir*, vol. 26, no. 17, pp. 13883-13891, 2010.
- [10] A. Tserepi *et al.*, "Plasma Nanotextured Polymeric Surfaces for Controlling Cell Attachment and Proliferation: A Short Review," *Plasma Chemistry and Plasma Processing*, journal article vol. 36, pp. 107-120, 2015.
- [11] J. Shen and J. Kirschenr, "Tailoring magnetism in artificially structured materials: the new frontier," *Surface Science*, vol. 500, no. 1-3, pp. 300-322, 2002.
- [12] G. Costantini *et al.*, "Tuning surface reactivity by in situ surface nanostructuring," *Journal Of Chemical Physics*, vol. 112, no. 15, pp. 6840-6843, 2000.
- [13] N. Vourdas *et al.*, "Plasma directed assembly and organization: bottom-up nanopatterning using top-down technology," *Nanotechnology*, vol. 21, no. 8, p. 085302, 2010.
- [14] F. F. Chen and J. P. Chang, *Lecture notes on principles of plasma processing*. Plenum/Kluwer, 2002.
- [15] M. A. Lieberman and A. J. Lichtenberg, *Principles of Plasma Discharges and Materials Processing*, 2nd ed. Wiley, 2005.
- [16] C. Steinbruchel, "Universal energy dependence of physical and ion-enhanced chemical etch yields at low ion energy," *Appl. Phys. Lett.*, vol. 55, no. 19, pp. 1960-1962, 1989.
- [17] J. W. Coburn and H. F. Winters, "Ion- and electron-assisted gas-surface chemistry. An important effect in plasma etching," *Journal Of Applied Physics*, vol. 50, no. 5, p. 3189, 1979.
- [18] J. D. Plummer, M. Deal, and P. B. Griffin, *Silicon VLSI Technology. Fundamentals, Practice and Modeling*. New Jersey: Prentice Hall, 2000.
- [19] G. Kokkoris and E. Gogolides, "The potential of ion-driven etching with simultaneous deposition of impurities for inducing periodic dots on surfaces," *Journal of Physics D: Applied Physics*, vol. 45, no. 16, p. 165204, 2012.
- [20] G. Kokkoris, V. Constantoudis, P. Angelikopoulos, G. Boulousis, and E. Gogolides, "Dual nanoscale roughness on plasma-etched Si surfaces: Role of etch inhibitors," *Physical Review B - Condensed Matter and Materials Physics*, vol. 76, no. 19, p. 193405, 2007.
- [21] V. Constantoudis, G. Kokkoris, and E. Gogolides, "Three-dimensional geometrical modeling of plasma transfer effects on line edge roughness: Comparison with experiments and rules of thumb," *Journal of Micro/ Nanolithography, MEMS, and MOEMS*, vol. 12, no. 4, p. 041310, 2013.
- [22] G. Kokkoris, V. Constantoudis, and E. Gogolides, "Nanoscale Roughness Effects at the Interface of Lithography and Plasma Etching: Modeling of Line-Edge-Roughness Transfer During Plasma Etching," *Ieee Transactions On Plasma Science*, vol. 37, no. 9, pp. 1705-1714, 2009.
- [23] N. Nakazaki, H. Tsuda, Y. Takao, K. Eriguchi, and K. Ono, "Two modes of surface roughening during plasma etching of silicon: Role of ionized etch products," *Journal of Applied Physics*, vol. 116, no. 22, p. 223302, 2014.

- [24] R. Petri *et al.*, "Silicon Roughness Induced By Plasma-Etching," *Journal Of Applied Physics*, vol. 75, no. 11, pp. 7498-7506, 1994.
- [25] P. Brault, P. Dumas, and F. Salvan, "Roughness scaling of plasma-etched silicon surfaces," *Journal Of Physics-Condensed Matter*, vol. 10, no. 1, pp. L27-L32, 1998.
- [26] W. S. Hwang, B. J. Cho, D. S. H. Chan, S. W. Lee, and W. J. Yoo, "Effects of volatility of etch by-products on surface roughness during etching of metal gates in Cl₂," *Journal Of The Electrochemical Society*, vol. 155, no. 1, pp. H6-H10, 2008.
- [27] S. Kuo-Tung and W. P. Stella "Mass Spectrometry, Optical Emission Spectroscopy, and Atomic Force Microscopy Studies of Si Etch Characteristics in a Cl₂ Plasma Generated by an Electron Cyclotron Resonance Source," *Japanese Journal of Applied Physics*, vol. 33, no. 12S, p. 7112, 1994.
- [28] G. Boulousis, V. Constantoudis, G. Kokkoris, and E. Gogolides, "Formation and metrology of dual scale nano-morphology on SF₆ plasma etched silicon surfaces," *Nanotechnology*, vol. 19, no. 25, p. 255301, 2008.
- [29] Y. Yin and H. H. Sawin, "Surface roughening of silicon, thermal silicon dioxide, and low- k dielectric coral films in argon plasma," *Journal of Vacuum Science and Technology A: Vacuum, Surfaces and Films*, vol. 26, no. 1, pp. 151-160, 2008.
- [30] M. Martin and G. Cunge, "Surface roughness generated by plasma etching processes of silicon," *Journal of vacuum Science & Technology B*, vol. 26, no. 4, pp. 1281-1288, 2008.
- [31] K. J. Kanarik *et al.*, "Overview of atomic layer etching in the semiconductor industry," *Journal of Vacuum Science & Technology A: Vacuum, Surfaces, and Films*, vol. 33, no. 2, p. 020802, 2015.
- [32] J. A. Levinson, E. S. G. Shaqfeh, M. Balooch, and A. V. Hamza, "Ion-assisted etching and profile development of silicon in molecular and atomic chlorine," *Journal Of Vacuum Science & Technology B*, vol. 18, no. 1, pp. 172-190, 2000.
- [33] M. A. Vyvoda *et al.*, "Role of sidewall scattering in feature profile evolution during Cl₂ and HBr plasma etching of silicon," *Journal of Vacuum Science and Technology B: Microelectronics and Nanometer Structures*, vol. 18, no. 2, p. 820, 2000.
- [34] E. S. G. Shaqfeh and C. W. Jurgensen, "Simulation Of Reactive Ion Etching Pattern Transfer," *Journal Of Applied Physics*, vol. 66, no. 10, pp. 4664-4675, 1989.
- [35] S. Hamaguchi, M. Dalvie, R. T. Farouki, and S. Sethuraman, "A Shock-Tracking Algorithm For Surface Evolution Under Reactive-Ion Etching," *Journal Of Applied Physics*, vol. 74, no. 8, pp. 5172-5184, 1993.
- [36] D. J. Cooperberg, V. Vahedi, and R. A. Gottscho, "Semiempirical profile simulation of aluminum etching in Cl-₂/BCl₃ plasma," *Journal Of Vacuum Science & Technology A-Vacuum Surfaces And Films*, vol. 20, no. 5, pp. 1536-1556, 2002.
- [37] G. Kokkoris, A. Tserepi, A. G. Boudouvis, and E. Gogolides, "Simulation of SiO₂ and Si feature etching for microelectronics and microelectromechanical systems fabrication: A combined simulator coupling modules of surface etching, local flux calculation, and profile evolution," *Journal of Vacuum Science and Technology A*, vol. 22, no. 4, pp. 1896-1902, 2004.
- [38] S. Osher and J. A. Sethian, "Fronts Propagating With Curvature-Dependent Speed - Algorithms Based On Hamilton-Jacobi Formulations," *Journal Of Computational Physics*, vol. 79, no. 1, pp. 12-49, 1988.
- [39] D. Adalsteinsson and J. A. Sethian, "A level set approach to a unified model for etching, deposition, and lithography II. 3-dimensional simulations," *Journal Of Computational Physics*, vol. 122, no. 2, pp. 348-366, 1995.
- [40] D. F. Richards, M. O. Bloomfield, S. Sen, and T. S. Cale, "Extension velocities for level set based surface profile evolution," *Journal Of Vacuum Science & Technology A*, vol. 19, no. 4, pp. 1630-1635, 2001.
- [41] A. P. Mahorowala and H. H. Sawin, "Etching of polysilicon in inductively coupled Cl-₂ and HBr discharges. III. Photoresist mask faceting, sidewall deposition, and microtrenching," *Journal Of Vacuum Science & Technology B*, vol. 20, no. 3, pp. 1077-1083, 2002.
- [42] Y. Osano and K. Ono, "An atomic scale model of multilayer surface reactions and the feature profile evolution during plasma etching," *Japanese Journal Of Applied Physics Part 1-Regular Papers Brief Communications & Review Papers*, Article vol. 44, no. 12, p. 8650, 2005.
- [43] Y. Zhang, C. Huard, S. Sriraman, J. Belen, A. Paterson, and M. J. Kushner, "Investigation of feature orientation and consequences of ion tilting during plasma etching with a three-dimensional feature profile simulator," *Journal of Vacuum Science & Technology A: Vacuum, Surfaces, and Films*, vol. 35, no. 2, p. 021303, 2017.
- [44] P. Xydi, "Simulation of topography evolution during plasma etching using the Narrow Band Level Set method," Master, Department of Informatics, Institute of Microelectronics, University of Athens, NCSR Demokritos, Athens, 2006.
- [45] A. P. Mahorowala and H. H. Sawin, "Etching of polysilicon in inductively coupled Cl-₂ and HBr discharges. II. Simulation of profile evolution using cellular representation of feature composition

- and Monte Carlo computation of flux and surface kinetics," *Journal Of Vacuum Science & Technology B*, vol. 20, no. 3, pp. 1064-1076, 2002.
- [46] W. Guo, B. Bai, and H. H. Sawin, "Mixing-layer kinetics model for plasma etching and the cellular realization in three-dimensional profile simulator," *Journal Of Vacuum Science & Technology A*, vol. 27, no. 2, pp. 388-403, 2009.
- [47] J. P. Chang, A. P. Mahorowala, and H. H. Sawin, "Plasma-surface kinetics and feature profile evolution in chlorine etching of polysilicon," *Journal Of Vacuum Science & Technology A-Vacuum Surfaces And Films*, Article vol. 16, no. 1, p. 217, 1998.
- [48] A. Sankaran and M. J. Kushner, "Integrated feature scale modeling of plasma processing of porous and solid SiO₂. I. Fluorocarbon etching," *Journal of Vacuum Science and Technology A: Vacuum, Surfaces and Films*, vol. 22, no. 4, p. 1242, 2004.
- [49] M. Wang and M. J. Kushner, "High energy electron fluxes in dc-augmented capacitively coupled plasmas. II. Effects on twisting in high aspect ratio etching of dielectrics," *Journal Of Applied Physics*, vol. 107, no. 2, p. 023309, 2010.
- [50] C. M. Huard, Y. Zhang, S. Sriraman, A. Paterson, K. J. Kanarik, and M. J. Kushner, "Atomic layer etching of 3D structures in silicon: Self-limiting and nonideal reactions," *Journal of Vacuum Science & Technology A: Vacuum, Surfaces, and Films*, vol. 35, no. 3, p. 031306, 2017.
- [51] J. T. Drotar, Y. P. Zhao, T. M. Lu, and G. C. Wang, "Surface roughening in shadowing growth and etching in 2+1 dimensions," *Physical Review B*, vol. 62, no. 3, pp. 2118-2125, 2000.
- [52] Y. P. Zhao, J. T. Drotar, G. C. Wang, and T. M. Lu, "Roughening in plasma etch fronts of Si(100)," *Physical Review Letters*, vol. 82, no. 24, pp. 4882-4885, 1999.
- [53] Y. Osano and K. Ono, "Atomic-scale cellular model and profile simulation of poly-Si gate etching in high-density chlorine-based plasmas: Effects of passivation layer formation on evolution of feature profiles," *Journal of Vacuum Science and Technology B: Microelectronics and Nanometer Structures*, vol. 26, no. 4, pp. 1425-1439, 2008.
- [54] H. Tsuda, H. Miyata, Y. Takao, K. Eriguchi, and K. Ono, "Three-Dimensional Atomic-Scale Cellular Model and Feature Profile Evolution during Si Etching in Chlorine-Based Plasmas: Analysis of Profile Anomalies and Surface Roughness," *Japanese Journal Of Applied Physics*, vol. 50, no. 8, p. 08JE06, 2011.
- [55] H. Tsuda, Y. Takao, K. Eriguchi, and K. Ono, "Modeling and simulation of nanoscale surface rippling during plasma etching of Si under oblique ion incidence," *Japanese Journal of Applied Physics*, vol. 51, no. 8 PART 2, 2012, Art. no. 08hc01.
- [56] H. Tsuda, N. Nakazaki, Y. Takao, K. Eriguchi, and K. Ono, "Surface roughening and rippling during plasma etching of silicon: Numerical investigations and a comparison with experiments," *Journal of Vacuum Science and Technology B: Microelectronics and Nanometer Structures*, vol. 32, no. 3, p. 031212, 2014, Art. no. 031212.
- [57] M. Tuda, K. Nishikawa, and K. Ono, "Numerical study of the etch anisotropy in low-pressure, high-density plasma etching," *Journal Of Applied Physics*, vol. 81, no. 2, pp. 960-967, 1997.
- [58] O. Yugo, M. Masahito, I. Naoshi, T. Kazuo, E. Koji, and O. Kouichi, "A Model Analysis of Feature Profile Evolution and Microscopic Uniformity during Polysilicon Gate Etching in Cl₂/O₂ Plasmas," *Japanese Journal of Applied Physics*, vol. 45, no. 10S, p. 8157, 2006.
- [59] E. A. Ogryzlo, D. E. Ibbotson, D. L. Flamm, and J. A. Mucha, "Doping and crystallographic effects in Cl-atom etching of silicon," *Journal of Applied Physics*, vol. 67, no. 6, p. 3115, 1990.
- [60] N. Nakazaki, H. Matsumoto, H. Tsuda, Y. Takao, K. Eriguchi, and K. Ono, "Surface smoothing during plasma etching of Si in Cl₂," *Applied Physics Letters*, vol. 109, no. 20, p. 204101, 2016.
- [61] W. Guo and H. H. Sawin, "Modeling of the angular dependence of plasma etching," *Journal Of Vacuum Science & Technology A*, vol. 27, no. 6, pp. 1326-1336, 2009.
- [62] S. Mouchtouris and G. Kokkoris, "Multiscale Modeling of Low Pressure Plasma Etching Processes: Linking the Operating Parameters of the Plasma Reactor with Surface Roughness Evolution," *Plasma Processes and Polymers*, vol. 14, p. 1600147, 2017.
- [63] J. F. Ziegler, M. D. Ziegler, and J. P. Biersack, "SRIM – The stopping and range of ions in matter (2010)," *Nuclear Instruments and Methods in Physics Research Section B: Beam Interactions with Materials and Atoms*, vol. 268, no. 11–12, pp. 1818-1823, 2010.
- [64] A. L. Barabasi and H. E. Stanley, *Fractal Concepts in Surface Growth*. Cambridge University Press, 1995.
- [65] J. A. Sanchez-Garcia, L. Vazquez, R. Gago, A. Redondo-Cubero, J. M. Albella, and Z. Czigany, "Tuning the surface morphology in self-organized ion beam nanopatterning of Si(001) via metal incorporation: from holes to dots," *Nanotechnology*, vol. 19, no. 35, p. 355306, 2008.
- [66] B. Ziberi, M. Cornejo, F. Frost, and B. Rauschenbach, "Highly ordered nanopatterns on Ge and Si surfaces by ion beam sputtering," *Journal Of Physics-Condensed Matter*, vol. 21, no. 22, p. 224003, 2009.

- [67] J. Zhou, S. Facsko, M. Lu, and W. Moller, "Nanopatterning of Si surfaces by normal incident ion erosion: Influence of iron incorporation on surface morphology evolution," *Journal Of Applied Physics*, vol. 109, no. 10, p. 104315, 2011.
- [68] B. Ziberi, F. Frost, and B. Rauschenbach, "Self-organized dot patterns on Si surfaces during noble gas ion beam erosion," *Surface Science*, vol. 600, no. 18, pp. 3757-3761, 2006.
- [69] Y. Zhao, G. C. Wang, and T. M. Lu, *Experimental methods in the physical sciences. Vol. 37. Characterization of amorphous and crystalline rough surface: Principles and applications*. Academic Press, 2001.